<u>IRA (I) – ISAC (I)– Ostfold College of Engineering (N)</u>

Low power pulsed radar for induced atmospheric phenomena investigation

(IRA –Italy-) S. Montebugnoli, A. Cattani, C. Bortolotti, F. Fiocchi, F. Liberati, J. Monari, A. Maccaferri, S. Mariotti, A. Orlati, F. Perini, S. Righini, M. Poloni, M. Roma, A. Scalambra, M. Teodorani, Tittarelli F. F.
(ISAC –Italy-)G. Cevolani, G. Bortolotti G. Pupillo, G. Trivellone
(OCE –Norway-) B.G.Hauge, E. P. Strand

IRA 321/02

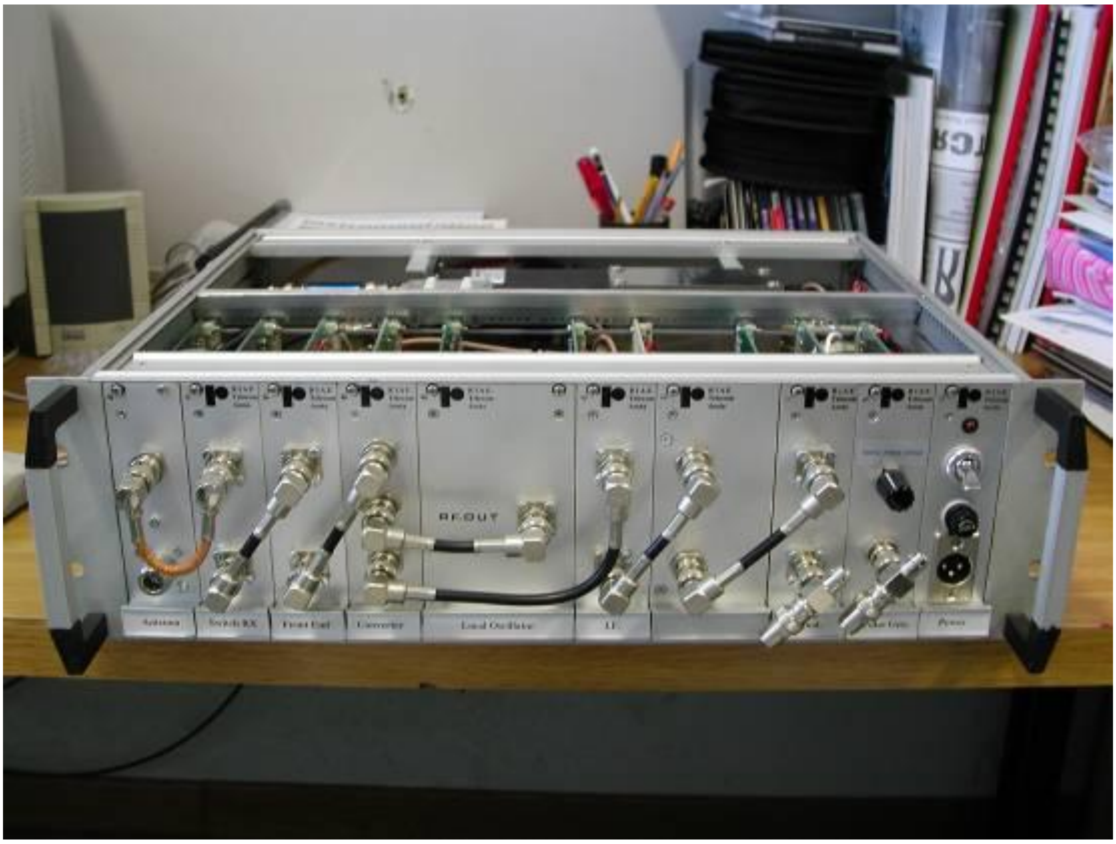

…..let us start with some pictures of the system……..

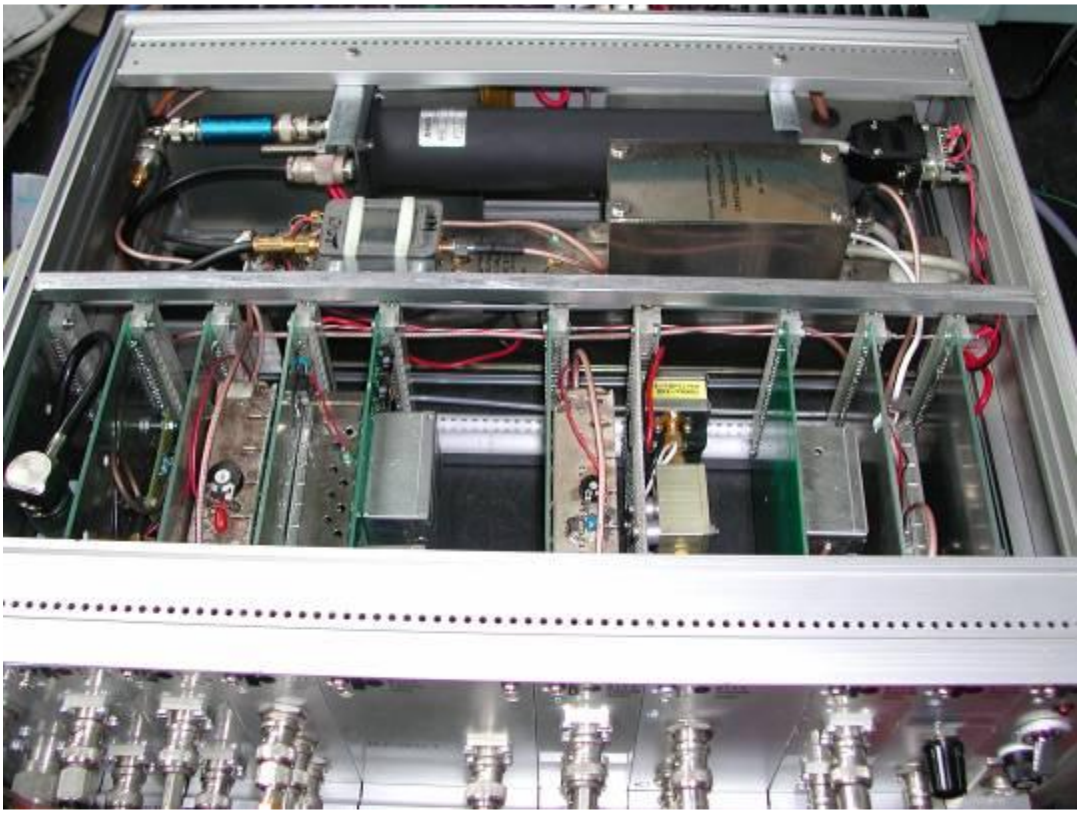

Introduction

An UHF low power portable pulsed radar, for research activities, is here presented. With the described equipment, small meteoroids, diminutive artificial space debris entering the high layers of the atmosphere and many other atmospheric phenomena, can be investigated. As it will be shown, the use of UHF radars is widely extended also to extremely important civil and military applications. The equipment has been developed as a collaboration among the *CNR Institute of Radioastronomy* (IRA –Bo-, Italy), the *CNR-ISAC Institute* (Bo, Italy) and the *Sarpsborg Ostfold College of Engineering* (Norway). The CNR IRA is involved in astrophysical researches in the radio field and transfers its expertise in radio engineering to the mentioned collaboration. The CNR-ISAC Institute continuously monitors, with the Bologna–Lecce bistatic radar, small meteoroids and, when possible, detects and controls some artificial debris that enter the high atmosphere of our planet. The *Ostfold College* is engaged, since 1984, in an intriguing and extremely interesting research concerning plasma-like ball lights, reaching 30 mt in diameter, that appear and sometime move at very high velocity in Hessdalen (Norway). Their scientific explanation, target of the ongoing research into the valley, is still unknown. The phenomenon being investigated is a physical light phenomenon that has absolutely nothing to do with any other “exotic” argument. Due to the fact that these different researches can be faced with the same observation methods, a cooperation between the three institutions, oriented to the design of such kind of radar, has been formalised.

1. Scientific Rationale

The system has been designed and developed to better fit the observing demands imposed by the monitoring and target distance measuring activities in both the above mentioned programs, but it is also interesting to underline how wide are the applications of UHF radar in other civil and military fields. New applications of these type of UHF radar continuously come out in many science branches and also in our everyday life.

ATMOSPHERIC OBSERVATIONS

The 420-450 MHz band is excellent for long-range search and surveillance and, to a lesser extent, target tracking. The large antennas required to achieve a good angular resolution generally limit operations to land or ship-based installations. The 449 MHz frequency is allocated to wind profiler radars that measure the atmosphere specifically near the Earth surface. The radars measure wind speed and direction as a function of time and altitude, an information that is useful to aviation. NOAA is planning a network to cover the United States. Here follows (FIG.1.1) a standard NOAA wind profile display

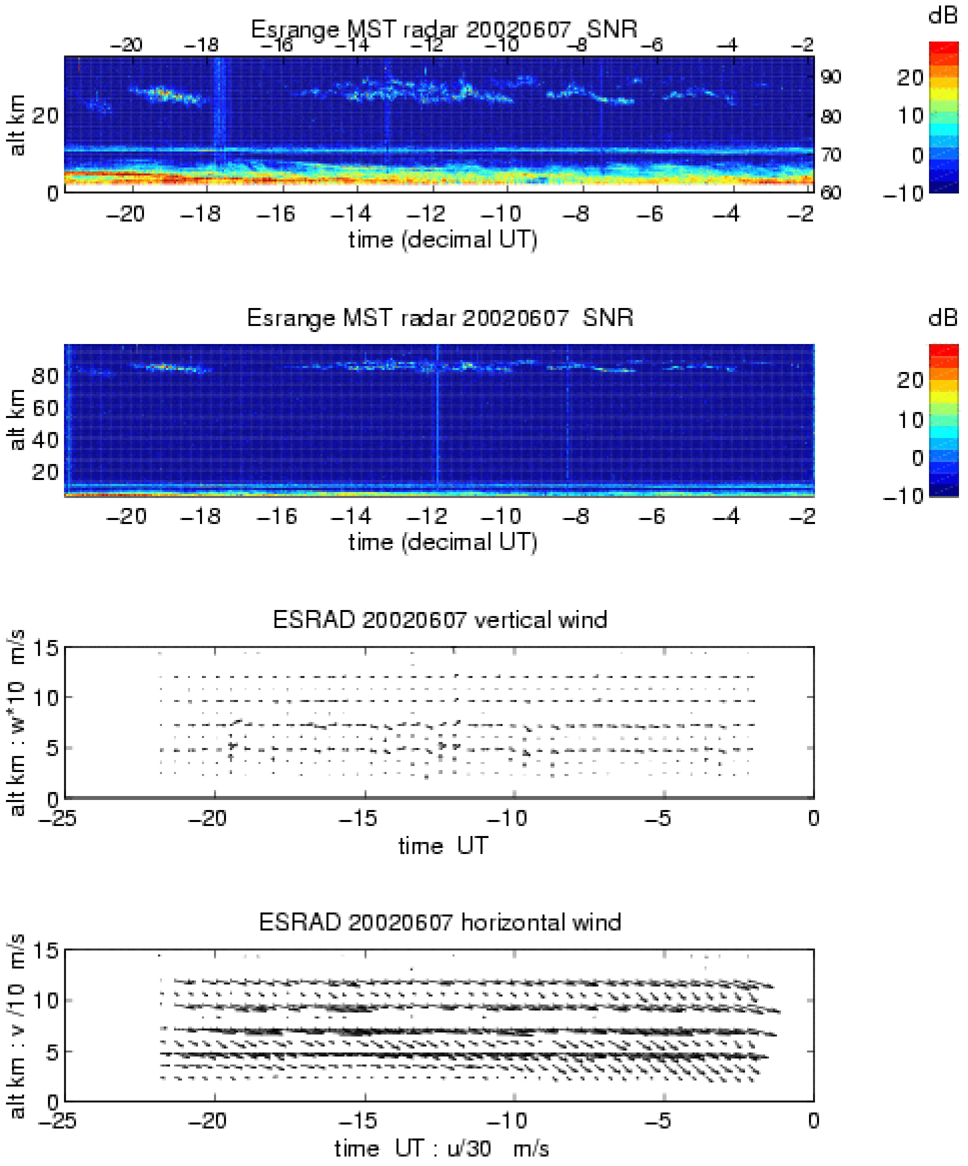

FIG.1.1 NOAA wind profile example of data displaying (*source: NOAA Web page*)

Radar wind profilers are instruments which measure wind speeds and other related parameters within the atmosphere over a relatively deep region (FIG.1.2). Depending on the frequency and power being used, this height region could cover an altitude range of typically 400 mt-10/15 km, reaching even 25 km when using the most powerful radars. Unlike the more widely known weather radars, wind profilers use near-vertical radar beams. While weather radars can measure atmospheric motion up to ranges of 100-200 km, these measurements are restricted to those areas where precipitations occur, or occasionally clear-air targets can be spotted: the lowest 1-2 km of the atmosphere. When wind measurements are possible, often only the radial wind component can be directly measured. Wind profiler radars, on the other hand, are designed to measure the wind vectors, and other pertinent atmospheric parameters, immediately above the site. Their specialities include their height coverage, their ability to determine both vertical and horizontal wind vectors, and their capability to monitor motions with high temporal resolution from heights close to the ground and into the upper troposphere and stratosphere during all conditions, including clean-air.

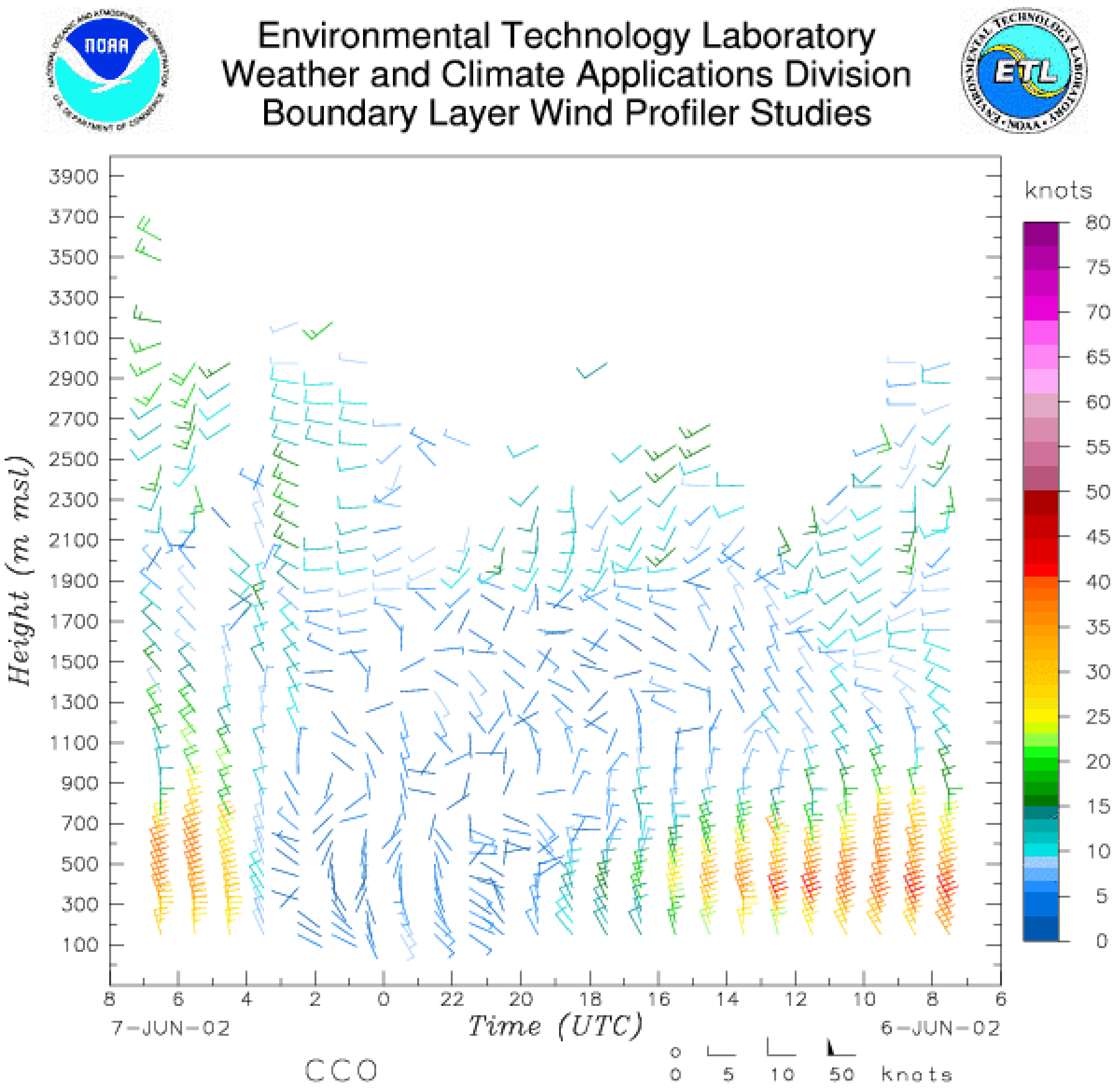

FIG.1.2 Another example of NOAA wind profile (*source: NOAA Web page*)

They can even measure turbulence strength. They are also known as MST (Meso-Strato-Troposphere) radars because of their ability to measure winds in the mesosphere, stratosphere, and troposphere. The most powerful of these radars can make useful measurements up to about a 25 km altitude, but also between 60 km and 90 km. In the troposphere and stratosphere, the unhomogeneity responsible for the radar scatter can be generated by turbulent mixing of existing temperature and humidity gradients, while in the mesosphere they are generated primarily by the mixing of existing large-scale electron density gradients, e.g. generated by ablation of meteoroids. A recent review of these radars can be found in (*Hocking, Radio Science, vol. 32, pp2241-2270, (1997)).* Within the USA, a network of profilers has been established by NOAA (National Oceanic and Atmospheric Administration), using a frequency in the 400-500 MHz band. However, this choice of frequency leads to contamination from other scattering targets like birds and insects, and can on occasion lead to incorrect interpretation of wind motions. In Europe, another network (CWINDE) has been established, but it is designed on a "contribution basis only" (FIG.1.3).

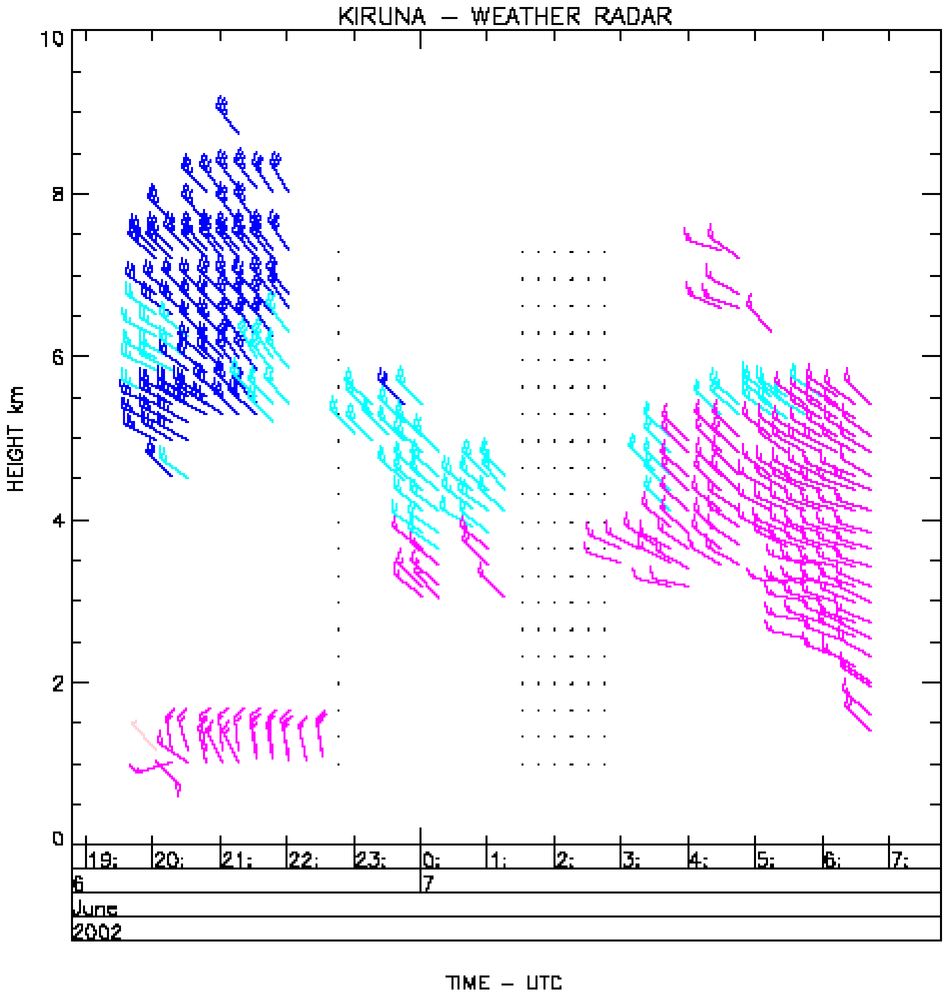

FIG.1.3 KIRUNA UHF Radar weather display example

OTHER USES in the 400-500 MHz band

A short report on the use of the UHF band in radar (monostatic and bistatic configuration) is here reported. Details on all the below reported applications are visible on their related web pages

The Air Force Ballistic Missile Early Warning System (BMEWS) has been the backbone of the U.S. missile defense system for over 30 years. The BMEWS radars are located in Clear, Alaska; Flyingdales, UK; and Thule and Sonderstrom AFB, Greenland, and are used for search and tracking. These radars operate in the 420-450 MHz band, and they have been modernised over the years. Technical improvements on the BMEWS radars may continue over the next 5-10 years. Spectrum requirements will continue over the next 10 years for the BMEWS. In the future, the BMEWS spectrum requirements for the 420-450 MHz band may be reduced if space-born radars can perform the early warning function. The Air Force Pave Paws, or AN/FPS-115, radars are used for detection and tracking of submarine launched ballistic missiles (SLBM), and for satellite tracking. Four phased array radars were installed between 1982 and 1987 in the United States. Other elements of the Pave Paws system are the Perimeter Acquisition Radar which was developed in the 1960's and 1970's as a Safeguard anti-ballistic missile (ABM) radar and the AN/FPS-85 SPACETRACK radar. The AN/FPS-115 Pave Paws radars and the Perimeter Acquisition Radar use the 420-450 MHz band, and are expected to operate for the next 10 years. The older AN/FPS-85 may be phased out. Some modernisation may occur to these radars, and the spectrum requirements will likely continue. The ship-born AN/SPS-40(V) is an older radar used by the Navy and USCG for air search and surveillance of air targets at long-ranges (FIG.1.4).

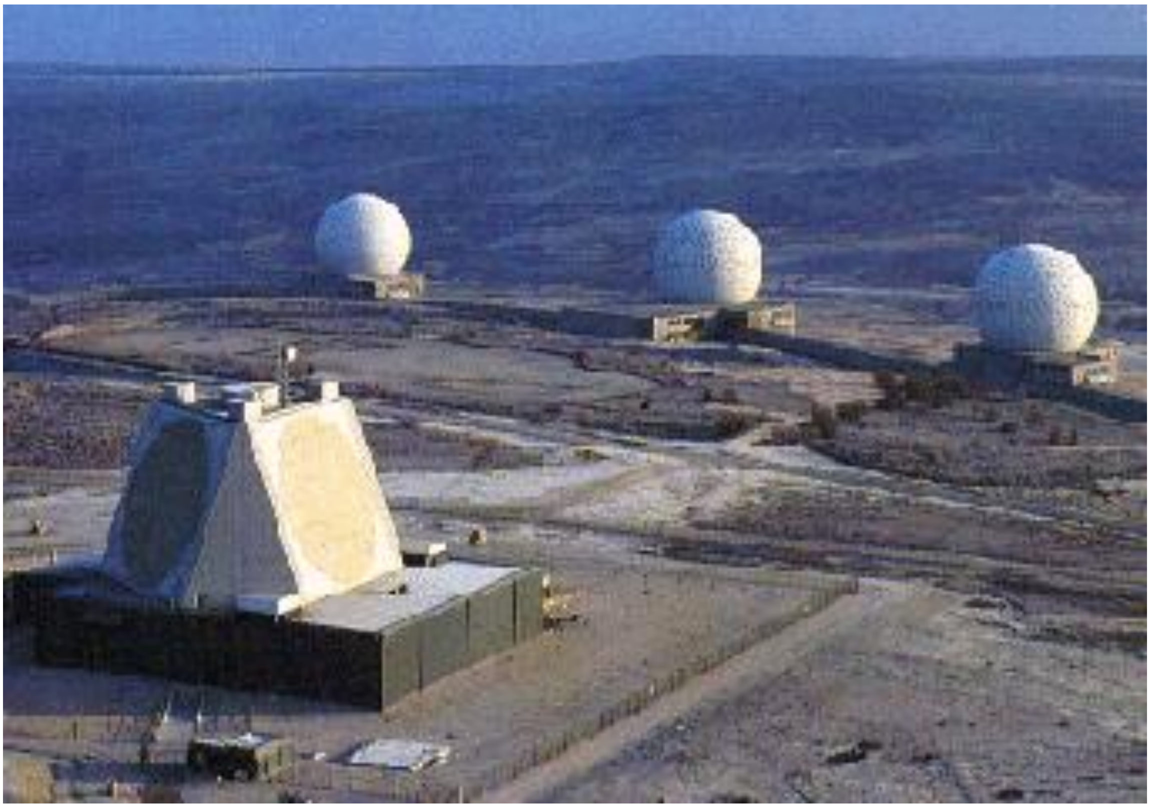

FIG.1.4 radar for air search and surveillance of air targets at long-ranges

The AN/SPS-40(V) radar has been updated, and it can be expected to be used for the next 10 years. The DOD indicated in its comments on our Inquiry that "[A]dvanced research in radiolocation is being performed in the bands ... 400-500; 390-940 MHz."[EN421] As discussed in the VHF sub-section, DOD has long-range spectrum requirements for UHF radars for anti-stealth and foliage penetration radars. When considering all of the classified and unclassified current and planned systems, it can be concluded that the military agencies are expected to continue their extensive use of the 420-450 MHz band for long-range search and surveillance radars for at least the next 10 years. The 500 MHz ESR (EISCAT Svalbard Radar) is owned by Finland, France, Germany, Great Britain, Japan, Norway and Sweden, to conduct ionospheric and magnetospheric studies in the auroral zone and polar cap areas (FIG.1.5). However, this radars have also been used for other purposes, such as studies of basic plasma physics phenomena, interplanetary scintillation, as astronomic VLBI stations, for upper atmosphere and meteor studies.

FIG. 1.5 EISCAT Svalbard Radar)

EMBLA PROJECT

A very interesting application of an UHF radar could be represented by the Hessdalen light phenomena investigation. The *Ostfold College of Engineering* (Sarpsborg University, in the Southern Norway) is engaged since 1984 in the search for a scientific explanation of one of the most intriguing light phenomena ever observed and investigated. At naked eye it appears as reported in FIG. 1.6, 1.7, 1.8

FIG.1.6: Light seen during winter time

Many theories refer to magnetic mono poles and/or Vorton effects but both of them seem (we are concerning with border physic concepts) to require an incredible amount of energy. Consequently, one of the target of the research is the comprehension of the origin of such a huge power. An automatic measuring station in the optical field (linked through the Internet to the University, has been installed in summer 1998. Many observations have been performed using extremely low frequency (ELF) receivers because it is well known that all the atmospheric phenomena are associated to the emission of ELF signals. A lot of data have been collected in this observing sessions.
An impressive number of videos and photos have been taken through the automatic video system installed in the valley by the Ostfold College. Some of these may be downloaded through the Internet, at the URL ***http://www.Hessdalen.org***

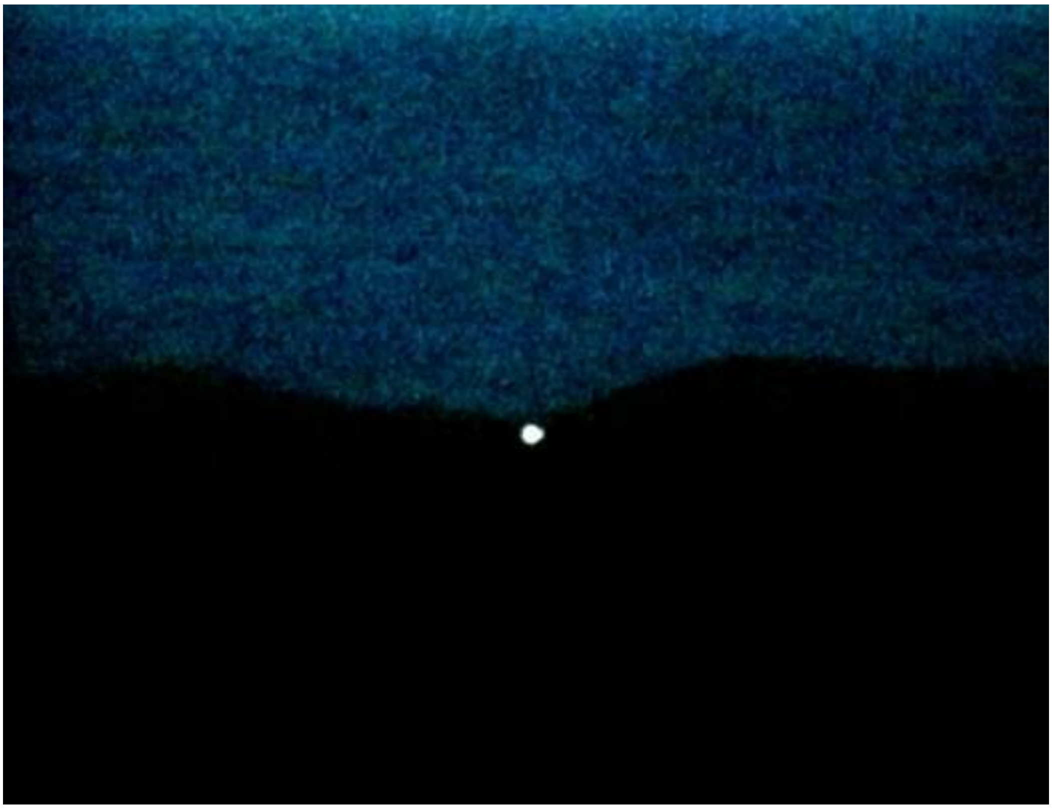

FIG.1.7: Image taken during the 2000 summer campaign

FIG.1.8 Image taken by the automatic video system installed in the valley

2. A little theory

Before describing the portable pulsed radar design, let us review some of the main concepts of radar theory that allow us to determine the system maximum range. Consider the simple configuration in FIG. 2.1

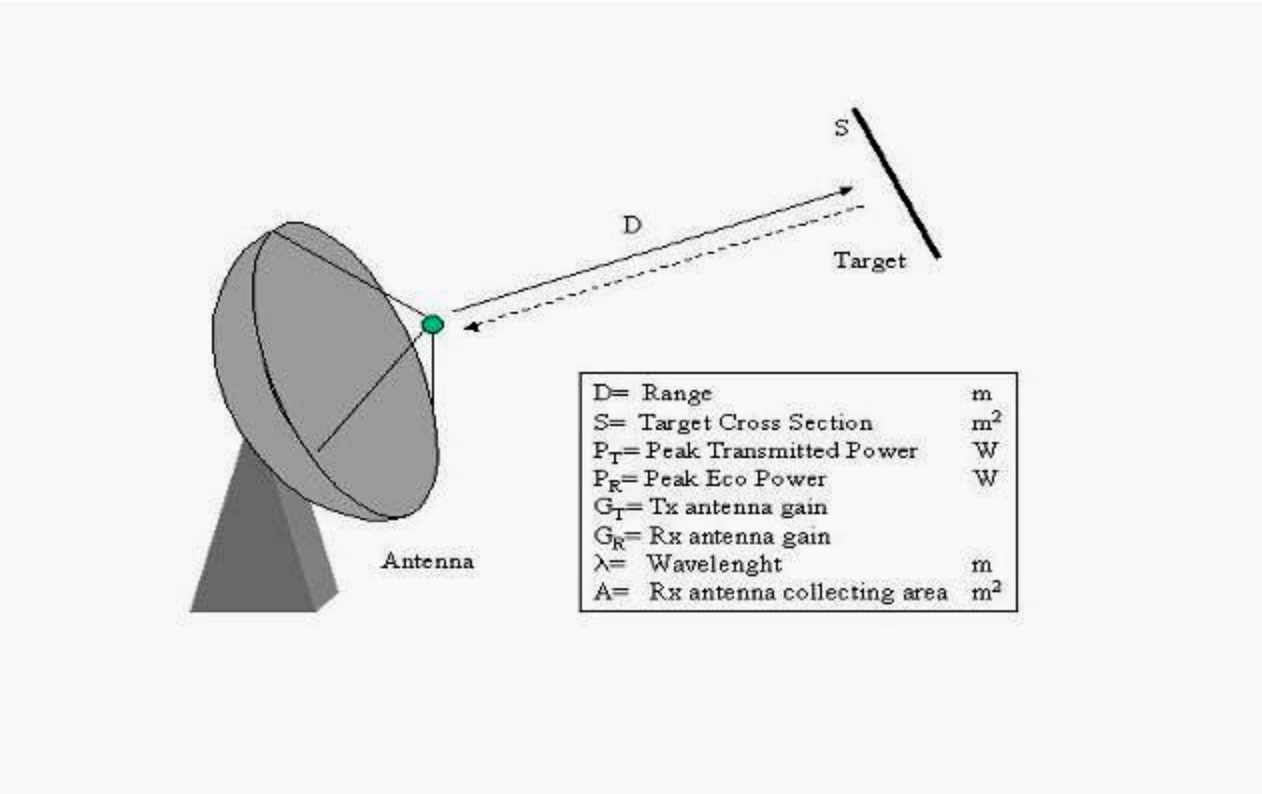

FIG. 2.1: Simple radar working scheme

The radiating power in the target direction is:

$$P_{RAD}= P_T G_T \qquad [W]$$

If D is the target distance, the surface of a sphere with the same radius D is:

$$S=4\pi D^2 \qquad [m^2]$$

So the power density per square meter at that distance (Poynting vector) is

$$\frac{P_T \cdot G_T}{4 \cdot \pi \cdot D^2} \qquad [W/ m^2]$$

If *s* is the equivalent area of the target that irradiates back the echo in all the directions, the target behaves as a new transmitting device (antenna) with transmitted power given by:

$$\frac{P_T \cdot G_T \cdot S}{4 \cdot \pi \cdot D^2} \qquad [W]$$

The electromagnetic signal bounced back from the target to the radar antenna (per square meter), is given by:

$$\frac{P_T \cdot G_T \cdot S}{4 \cdot \pi \cdot D^2} \cdot \frac{1}{4 \cdot \pi \cdot D^2} = \frac{P_T \cdot G_T \cdot S}{(4 \cdot \pi)^2 \cdot D^4} \qquad [\mathrm{W/m^2}]$$

The power “absorbed” by the radar antenna is proportional to the area:

$$A = \frac{G_R \cdot \lambda^2}{4 \cdot \pi} \qquad [\mathrm{m^2}]$$

therefore the power collected by the radar antenna is:

$$P_R = \frac{P_T \cdot G_T \cdot G_R \cdot S \cdot \lambda^2}{(4 \cdot \pi)^3 \cdot D^4} \qquad [\mathrm{W}]$$

In the case of a monostatic radar (the antenna is both transmitting and receiving) we can write :

$$G_T = G_R = \frac{4 \cdot \pi \cdot A}{\lambda^2}$$

so the received power is given by:

$$P_R = \frac{P_T \cdot A^2 \cdot S}{4 \cdot \pi \cdot D^4 \cdot \lambda^2} \qquad [\mathrm{W}]$$

We determine now the range of the radar taking in consideration that the echo is becoming weaker and weaker as the target distance D increases. The range is then limited by the sensitivity of the receiver. In this way if P_{MIN} is the minimum detectable power, D_{MAX} will represent the maximum range of the radar. The previous expression becomes:

$$P_{MIN} = \frac{P_T \cdot A^2 \cdot S}{4 \cdot \pi \cdot (D_{MAX})^4 \cdot \lambda^2} \qquad [\mathrm{W}]$$

Solving this last expression by D_{MAX} we obtain the range of the radar:

$$D_{MAX} = \sqrt[4]{\frac{P_T \cdot A^2 \cdot S}{4 \cdot \pi \cdot P_{MIN} \cdot \lambda^2}} \qquad [\mathrm{m}]$$

The above considerations are referred to a CW radar. In the case we want to detect and measure the distance of a target, we need to use a pulsed radar.

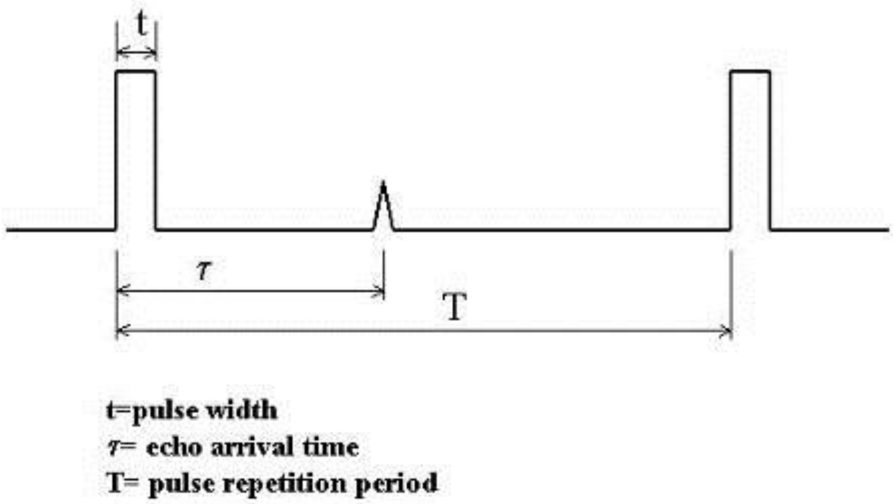

If *c* is the speed of light, *D* the distance of the target and τ is the elapsed time between the transmission and the received echo, the distance is given by :

$$D = \frac{c \cdot \tau}{2} \qquad [m]$$

A last consideration: after the emission of the pulse, the radar spends a bit of time "listening" to the echo. In other words the transmitter works only for the time "t" and therefore the average emitted power is much lower than the peak power.
For instance, if we have

t= 1 microsec. (pulse width)
T= 1 millisec. (repetition period)

The Duty Cycle becomes:

$$D.C. = \frac{t}{T} = \frac{1 \cdot 10^{-6}}{1 \cdot 10^{-3}} = 0{,}001$$

then the average transmitted power is:

$$P_m = P_p\ D.C \qquad \text{where } P_p = \text{Peak Power}$$

So, in this example the average transmitted power is 1000 times lower than the transmitted peak power. This is very important especially for portable systems due to the need to supply it with battery packs.

3. The IRA- ISAC- OCI Pulsed Radar

The goal of the collaboration is the design of a low power portable pulsed radar able to detect and measure the distance of any kind of targets or phenomena inside the atmosphere. The basic schematic diagram of the system is presented in FIG. 3.1

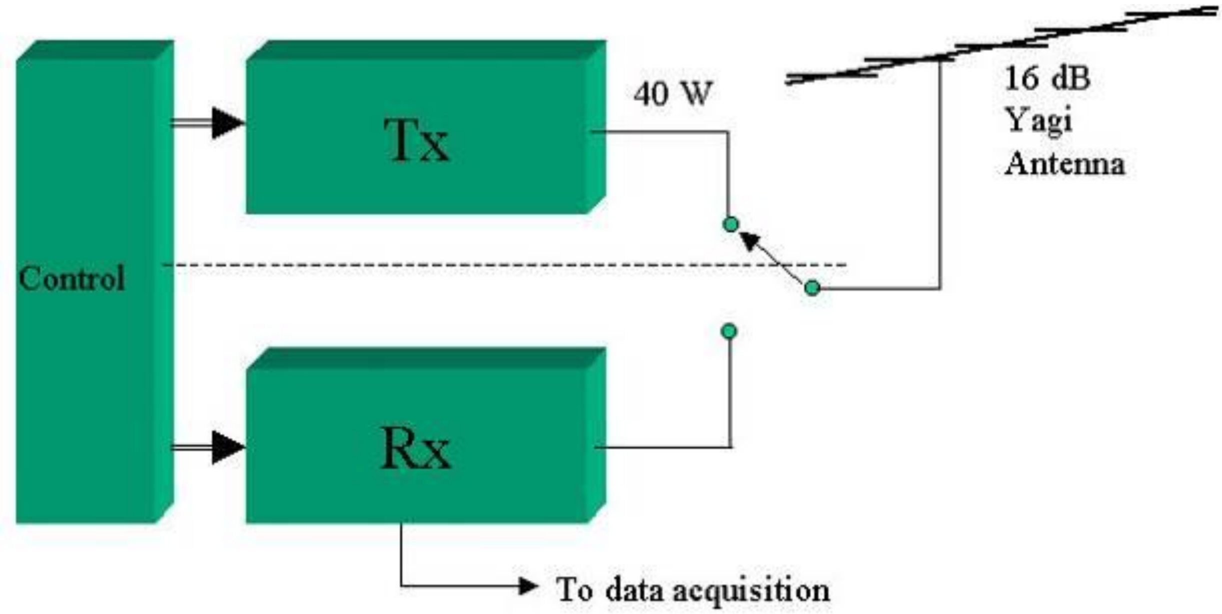

FIG. 3.1: Basic block diagram of a radar system

We use a P_P=40 W transmitter tuned at 439.3 MHz with a pulses timing configuration:

t=	4	µsec.	(pulse width)
T=	100 -200	µsec	(repetition period →selection 1 and 2)
T=	800	µsec	(minimum repetition period → selection 3)

as visible in FIG. 3.2. In this situation the blind zone (determined by the pulse width) is:

D_{MIN}= (4 x 10^{-6} x 300 x 10^{6}) / 2= 600 m

while the maximum target distance measurable without any ambiguity (D_{MAX}), is found using the expression:

$$D = \frac{c \cdot \tau}{2}$$

in which we consider τ=T:

D_{MAX}= (100 x 10^{-6} x 300 x 10^{6}) / 2= 15 Km → in the case T=100 μsec
D_{MAX}= (200 x 10^{-6} x 300 x 10^{6}) / 2= 30 Km → in the case T=200 μsec
D_{MAX}= (800 x 10^{-6} x 300 x 10^{6}) / 2= 120 Km→ in the case T=800 μsec

If the distance of the target is greater than the one corresponding to the interpulse time, we would get the echo after the second or third (and so on) pulse has already been transmitted, introducing ambiguity. For instance, in our practical case this ambiguity on the distance measure would be a multiple of 15 Km if the 100μsec was selected(FIG. 3.3).

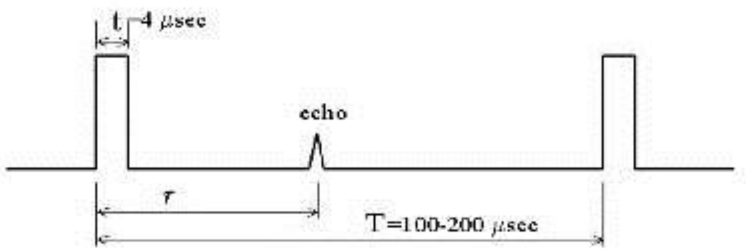

FIG. 3.2: Pulse timing in our system

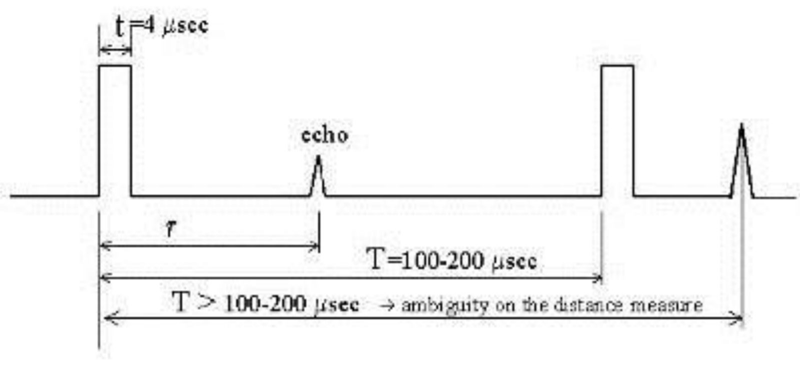

FIG. 3.3 Distance measure with a n x T μsec ambiguity

Concerning the average transmitted power we have:

$P_m = 40\ (4\ x10^{-6}\ /\ 100\ x\ 10^{-6}) = 1.6\ W$ → in the case T=100 μsec
$P_m = 40\ (4\ x10^{-6}\ /\ 200\ x\ 10^{-6}) = 0.8\ W$ → in the case T=200 μsec
$P_m = 40\ (4\ x10^{-6}\ /\ 800\ x\ 10^{-6}) = 0.2\ W$ → in the case T=800 μsec

This low consumption is very important for the portability of the system because it has to be supplied via a battery pack.

3.1 The Block Diagram

The block schematic diagram of the pulsed radar is reported below in FIG. 3.4.

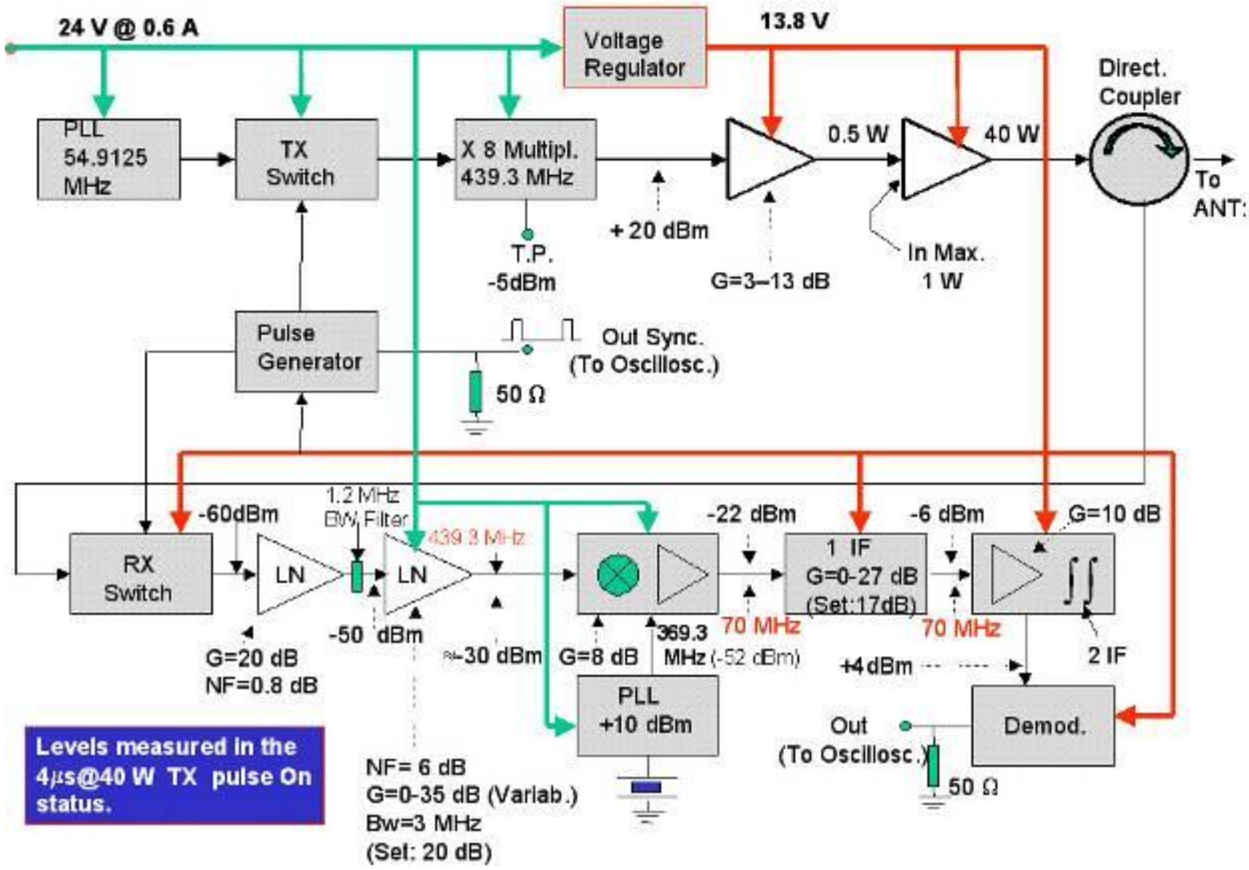

FIG. 3.4 Low power radar block diagram

The blocks composing the system are here briefly described:
<u>Transmitter:</u>

1- OSC----------- Hirshmann N.975 233, 54.9125 MHz Oven controlled quartz oscillator. Output power: +10 dBm

2- Tx Switch------- Mini Circuit PSW-1211, Switch TTL controllable.
Operating range: 10-2500 MHz,
Insertion loss:1.1 db (ON), 40 db (OFF)
Max. input level: +19 dBm (1 dB of compression)
Switching time: 4 μsec
Rise time. 2 μsec

3- X8 Multiplier--- Hirshmann VV42 B IVIV N 975 252
Output minimum level: +10 dBm

4- First P.A.------- Working freq. Range: 400/450
Efficiency: 40%
Gain: adjustable from 10 to 27 dB
Input max level: +10 dBm
Ouput max level: +37 dBm

5- Second P.A---- Working freq. Range: 400/450
Efficiency: 40%
Gain: adjustable from 3 to 17 dB
Input max level: +27 dBm
Ouput max level: +44 dBm
Tolerance on output 20:1 mismatchig: 5 seconds

<u>Receiver</u>

1- Circulator ------ Forem, Working band 400 – 470 MHz

2- Rx Swithc------ Mini Circuit Switch (ZFSW-2-46)
Operating range: DC – 4.6 GHz,
Insertion loss:1.2 db (ON), 40 db (OFF)
Max. input level: +27 dBm
Switching time: 4 μsec
Rise time. 2 μsec

3- PLL ------------- Local Oscillator (Oven Quartz ref. / PLL)
output freq.= 369.3 MHz
Max output level: +10 dBm

4- Front end------- LNA CNR Design,
G= 19 dB
NF= 0.65 dB
OIP3= +24 dBm

5- second LNA---- RIAE Amplifier, NF=6 dB
BW= 3 MHz
G= adjustable 1-36 db

6- Converter------- Mix + Amplif., G_{TOT}=8 dB
L.O level: +10dBm
Max. input level: +1 dBm
Conversion loss: 6.3 dB

7- first I.F Ampl.-- Max. input level : +13 dBm
NF: 3 dB
G: 27 dB

8- Sec. I.F Ampl.- G_{TOT}: 8 dB BW=1.2 MHz with SAW filter
8- Demod.--------- Custom circuit visible later in this paper
9- Sync. Gen.----- Custom circuit visible later in this paper

Block diagram description

A pulse generator is in charge to create the trigger pulses that, alternatively, make the system transmitting (for 4 μsec) and receiving (for 96, 194 or 796 μsec). While the system transmits, the receiver input stage (LN) is short circuited to the ground via a diode (Rx Switch block). In the receiver a LN amplifier (Front End) is used to dramatically reduce the noise figure. A cavity band pass filter (0.250 / 1 Megahertz of bandwidth with a little more than 1 dB of insertion loss) could be installed to increase the system sensitivity, in the point marked “ x ” between the two input LNAs. This will be evaluated, at the end of the design, with consideration on the global cost. After the down conversion to the I.F frequency (70 MHz) the signal is band pass filtered first with a 3 MHz wide BPF, amplified by the I.F amplifier and then filtered again with a narrow SAW filter, a FSMS0070A1 model. The I.F SAW Filter stage is visible in more details in FIG. 3.5

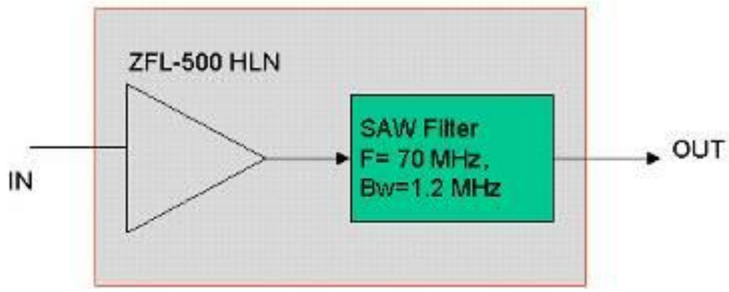

FIG. 3.5: SAW Filter stage

The SAW filter pin connections are reported in FIG.3.7 while the performances of the Minicircuit ZFL-500HLN amplifier are the following:

NF=5.3 dB
G=20 dB
F=0.05 – 500 MHz
DC= 15 V, 60 mA

A ZFL-500HLN amplifier was used for its very good performances and reliability as requested by the nature of the equipment working condition.
The signal, once detected, filtered and amplified in the demodulator block, is then sent to the Oscilloscope for the visualisation. A circulator is in charge to isolate the Tx and the Rx.
In order to make the system more suitable for measuring activities on the field, a battery power pack power supply is planned. In order to reduce the power consumption it is planned to disconnect the supply of the oven of the local oscillator. In this way a couple of hundreds of mA are saved.

In FIG. 3.6 it is reported a sketch of the front panel as it appears in practice.

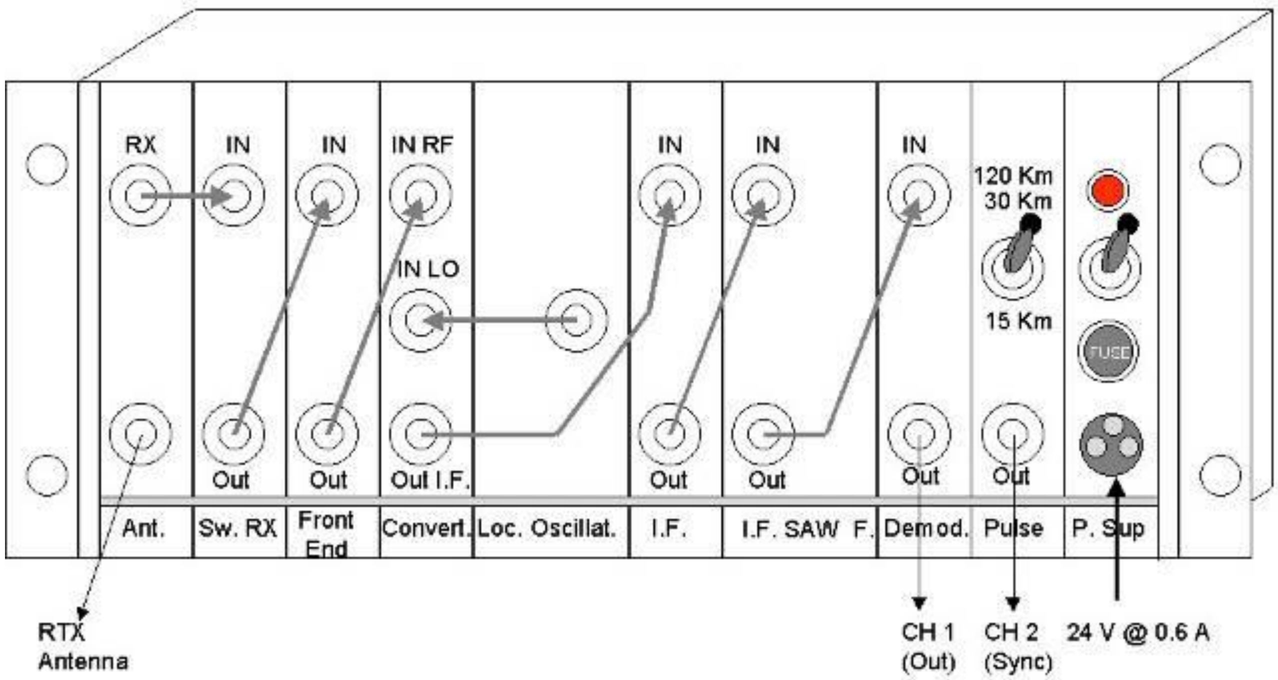

FIG. 3.6 Radar Front Panel

Many of the components of the equipment come from the Italian RIAE telecommunication Company, the remaining have been designed and assembled at the CNR laboratories.

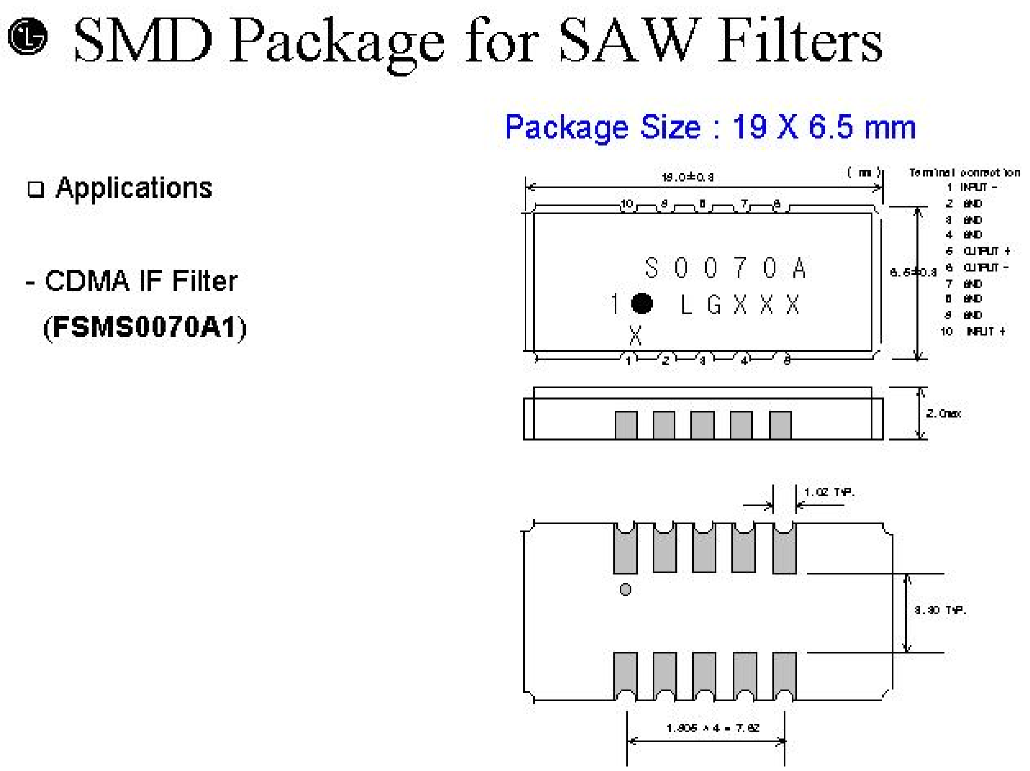

FIG. 3.7 Package of the SAW filter

The band of the FSMS0070A1 filter is visible in FIG. 3.8. The insertion loss of such a filter lies in the range 10-15 dB but in our case this doesn’t represent a problem because its position on the block schematic diagram is sufficiently far from the front –end. Since we detect the signal in the time domain, it is important to band limit the RF and the I.F signals in order to improve the sensitivity. As visible in FIG. 3.6, we introduce a 20 dB gain and high dynamic range Mini-circuit amplifier before the filter itself, in order to reduce, anyway, the insertion loss.

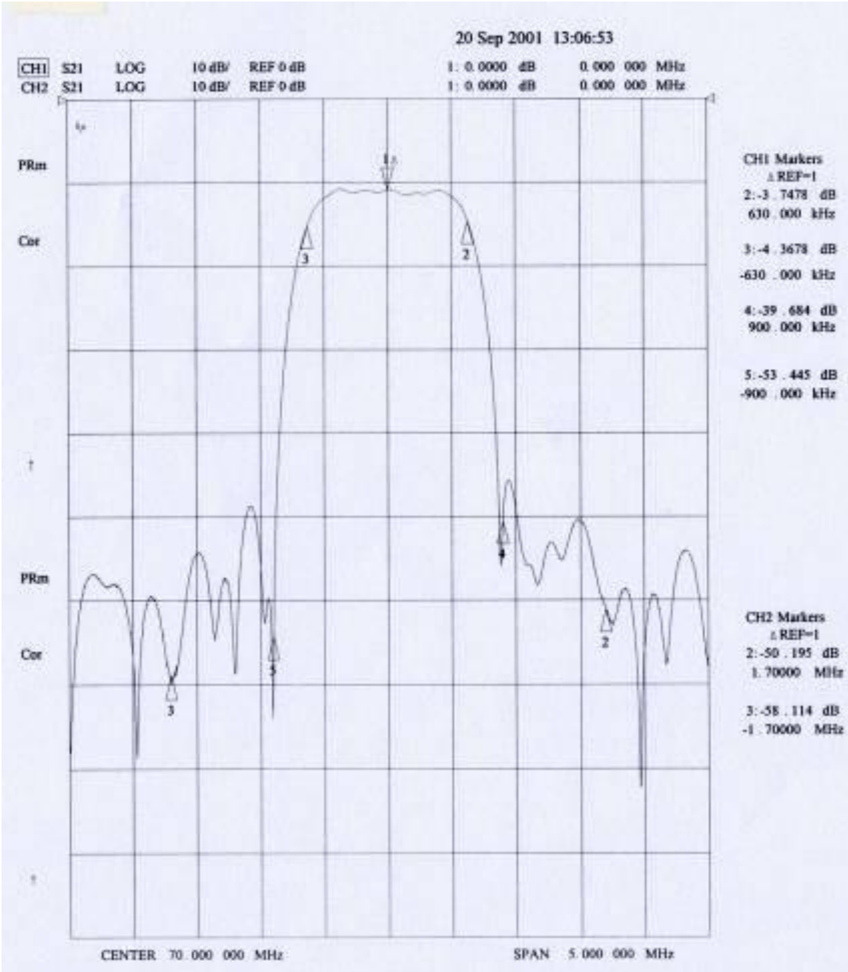

FIG. 3.8: Shape of the FSMS 0070A1, a 70 MHz - 1.2 MHz BW SAW filter

Concerning the timing of the system, in FIG. 3.9 the sequence of the pulses is presented. The sync pulse is 2 μsec wide and, due to various delays introduced by the different switches, the minimum time it needs to wait for the arrival of the first pulse is about 3.5 μsec. An ad hoc micro switch is installed on the sync block (Pulse block in FIG. 3.6) allowing the continuous transmission, at full power, in order to align the transmitting stages of the transmitter.

WARNING: in this phase it is compulsory to disconnect the receiver antenna cable from *RX* to *In* (blocks Ant. and Sw. Rx in FIG. 3.6). The full power, in this case, would burn the commutation diode at the Front End input. Care has also to be taken concerning the radar “output” stage and the “Yagi” antenna impedance matching. A high mismatch would cause a reflection of such a high power level to destroy the same switching diode at the front end input.

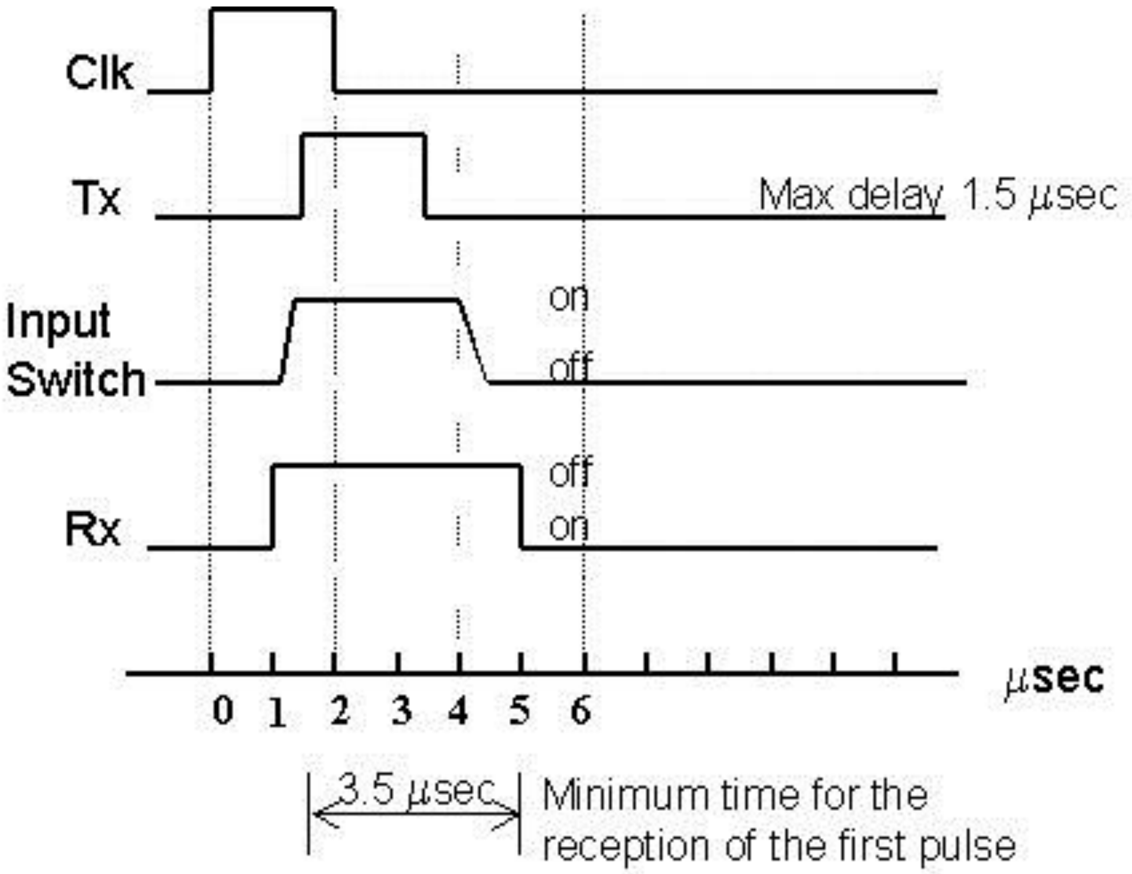

FIG. 3.9 Pulse Timing through the system

3.2 Electrical diagrams

We will describe with some details only the electrical schematic diagrams of some of the blocks of the radar. Some other blocks come from the RIAE telecommunication and many of them, in order to reduce the costs, result from the dismounting of commercial radio links systems under renewal. The same schematic diagram are printed in a more readable and enlarged version in the appendix of this paper

<u>3.2.0 RX- Switch</u>

This block is just after the TX-Rx antenna circular coupler. Two RF switches have been used in a cascade configuration in order to increase the isolation during the transmitter pulse On status. The electric schematic diagrams are reported in Appendix while a picture of the modules are shown in FIG. 3.10a,b. Here are clearly visible the TRACO DC-DC converters requested from both the Mini Circuit ZFSW-Z-46 and from the MACOM MA8430-2050 solid state switches. As already mentioned, the maximum input power allowed for this devices is +27 dBm

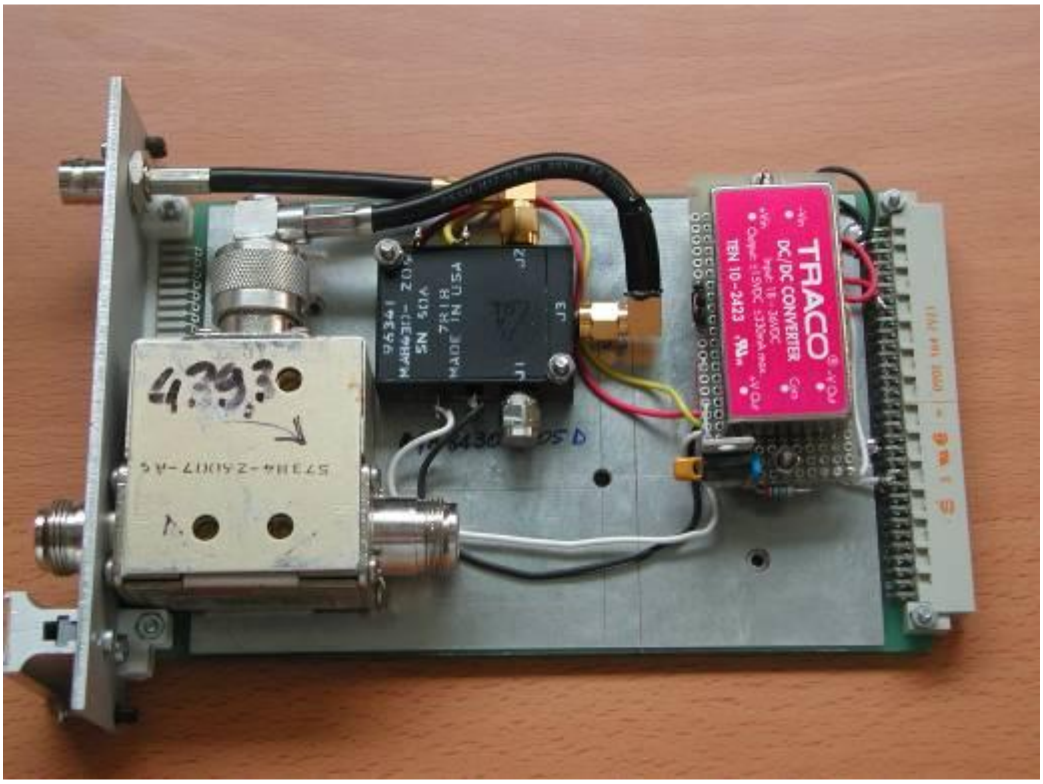

FIG. 3.10a First RX switch on board 1

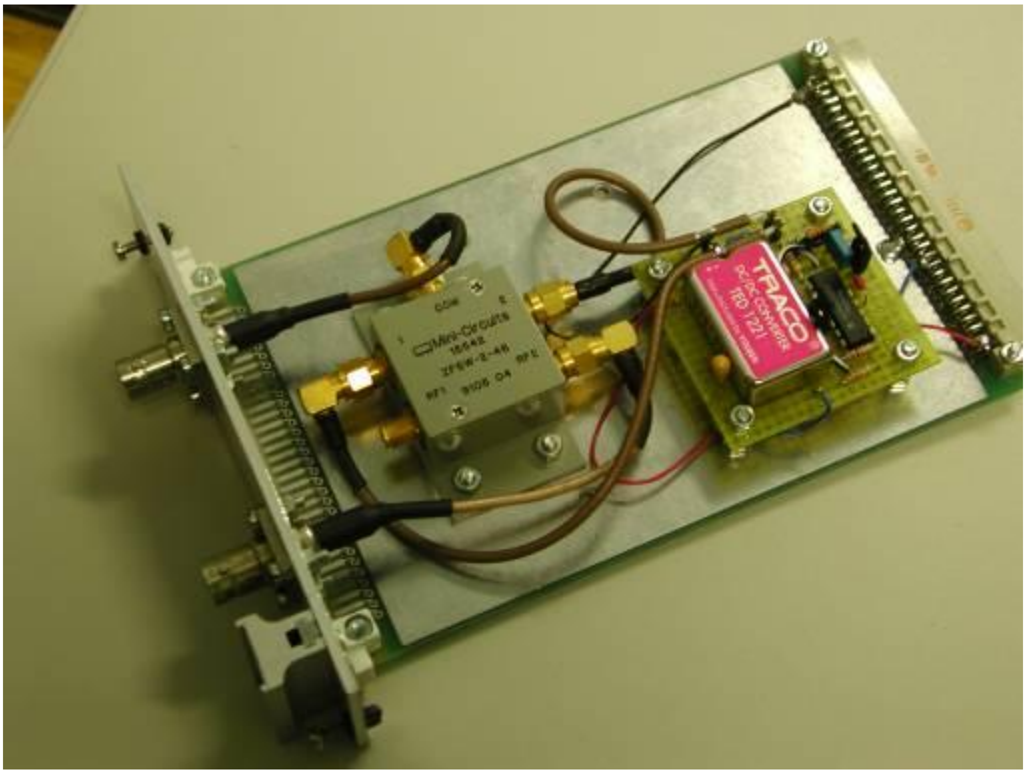

FIG. 3.10b Second RX switch on board 2

3.2.1- Front end

The Radar receiver front end comes from the prototype developed at the Medicina radiotelescopes labs for the Square Kilometre Array (SKA) consortium. Many efforts have been devoted to the design in order to reach very good performances at a very low cost (in SKA, at least one million of similar front ends will be required). The electric schematic diagram is presented in FIG. 3.11. A power Enhancement Pseudomorphic HEMPT (the ATF 54143 model designed for cellular phone base station) has been used. Since the LNA works at 12 V and the main voltage is 24/27 V, a voltage regulator is used to stabilise and obtain the requested 12V. The front end will decrease the noise figure from the 6 dB of the previous system version to less than 1 dB (0.6 / 0.7 dB). The front end has been assembled using very high Q components (high quality coils and capacitors). The here reported prototype is assembled on a FR4 substrate printed circuit board.

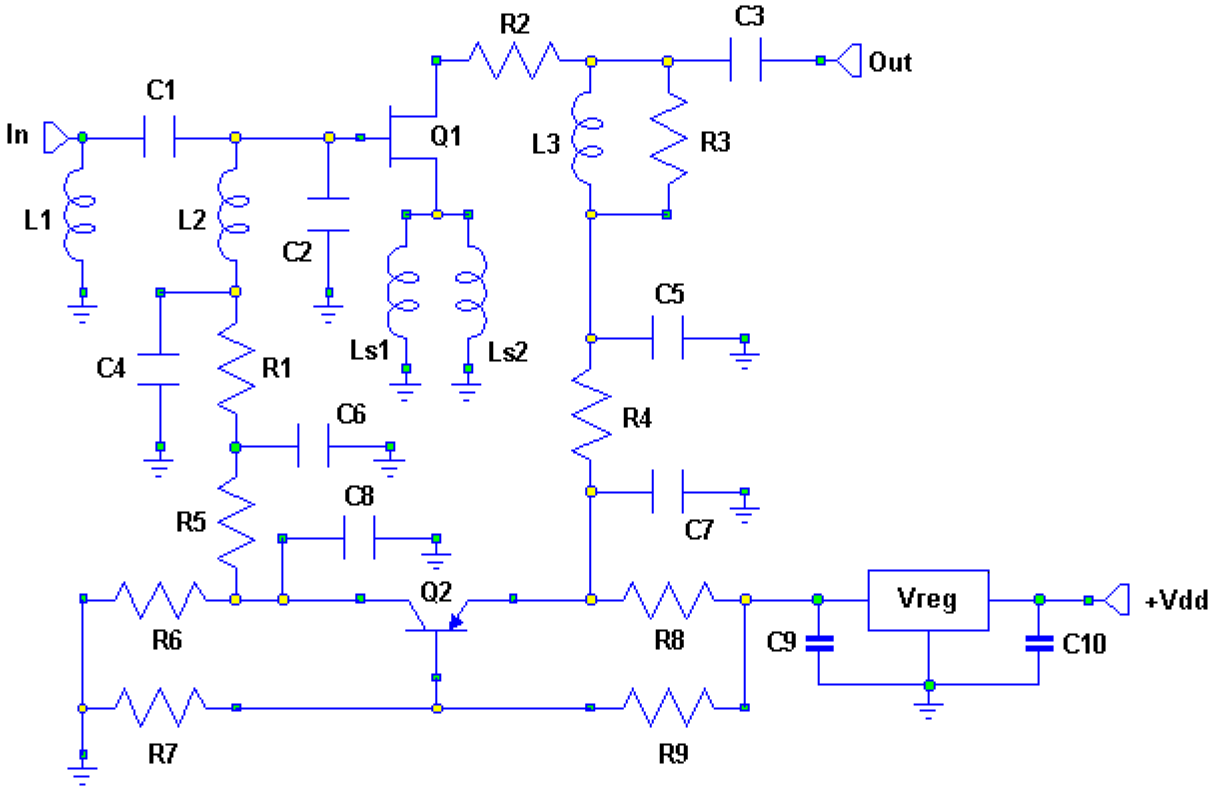

.

FIG.3.11 Front end Electrical diagram

List of components:

C1 = 7.5 pF ATC 100B7R5JP500X	R1 = 100 Ω RS	Q1 = Agilent ATF-54143
C2 = 1.2 pF ATC 100B1R2JP500X	R2 = 39 Ω RS	Q2 = Motorola 2N2907A
C3 = 33 pF ATC 100B330JP500X	R3 = 62 Ω RS	L1 = 220 nH Coilcraft 0805CS-221XJBC
C4 = 220 pF ATC 100B221KP200X	R4 = 12 Ω RS	
C5 = 220 pF ATC 100B221KP200X	R5 = 10 KΩ RS	L2 = 12.5 nH Coilcraft Mini Spring Air Core A04TJ
C6 = 10 nF AVX 12061C103KAT00J	R6 = 1 KΩ RS	

C7 = 10 nF AVX 12061C103KAT00J	R7 = 1 KΩ RS	
C8 = 10 nF AVX 12061C103KAT00J	R8 = 150 Ω RS	L3 = 47 nH Coilcraft Midi Spring Air Core 1812SMS-47NJ
C9 = 0.1 μF Ceramic Capacitor	R9 = 1.2 KΩ RS	
C10 = 0.33 μF Ceramic Capacitor		Vreg = ST L7812CV

As already mentioned, it presents a NF=0.65 dB with a very high dynamic range (OIP3= +24 dBm) at a G=19 dB. A picture of such a stage is visible in FIG. 3.12. The prototype has been assembled with surface mounting components in order to reduce the size. The circuit has been simulated with Microwave Office software package. The prototype in the figure satisfactorily fits the expected characteristics.

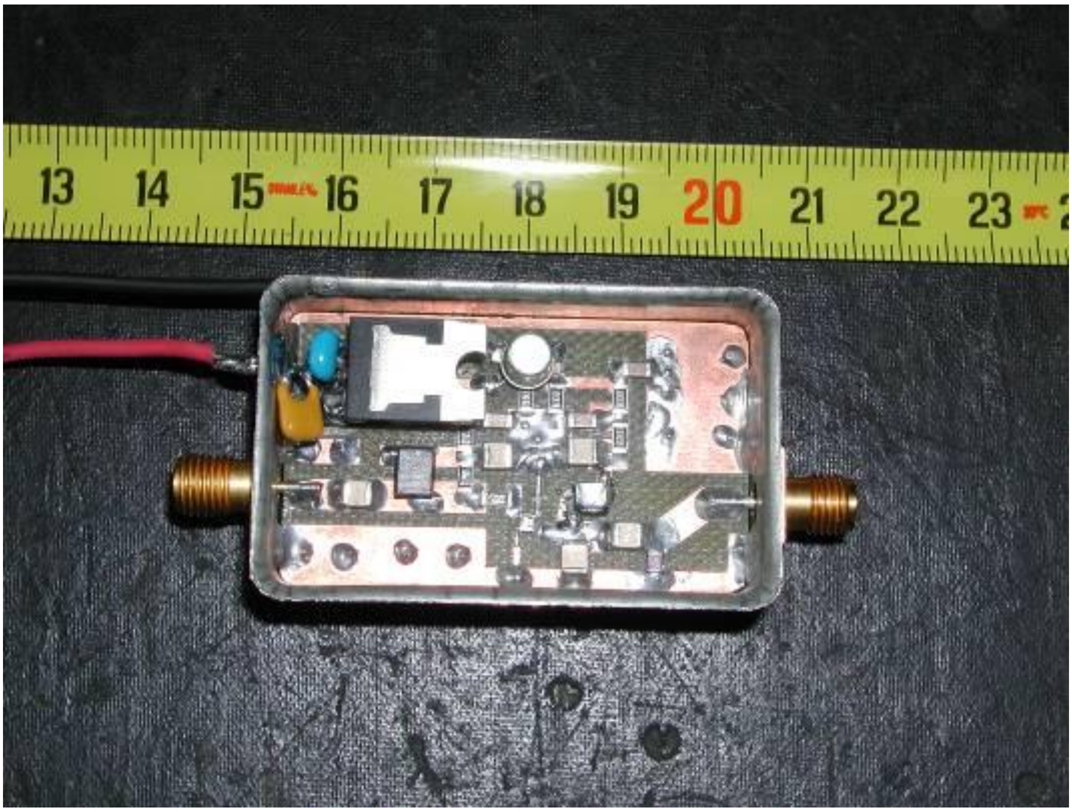

FIG.3.12 Radar Front End assembled prototype

3.2.2 – The pulse generator board

This board is in charge to generate the sync pulse with the proper width (≈ 4 μsec) and selectable repetition rate for the radar. Since a very stable pulse width and repetition rate are requested, the time base is equipped with a quartz oscillator (5120 KHz). After the generation, the signal is divided by different modules. With a 1 way, 3 positions selector, it is possible to choose 100, 200, 800 μsec in order to avoid ambiguities in the distance measures in the range 15, 30 and 120 Km respectively. The oscillator and divider is based on the 4060 chip. After some logic, the pulse is sent to the timing radar circuits as the PSW1211 Tx switch. The switch positioned in the point B is for continuous RF emission requested during servicing, as reported before in this paper. The electric circuit is presented in the Appendix while the picture of the module is visible in FIG.3.13

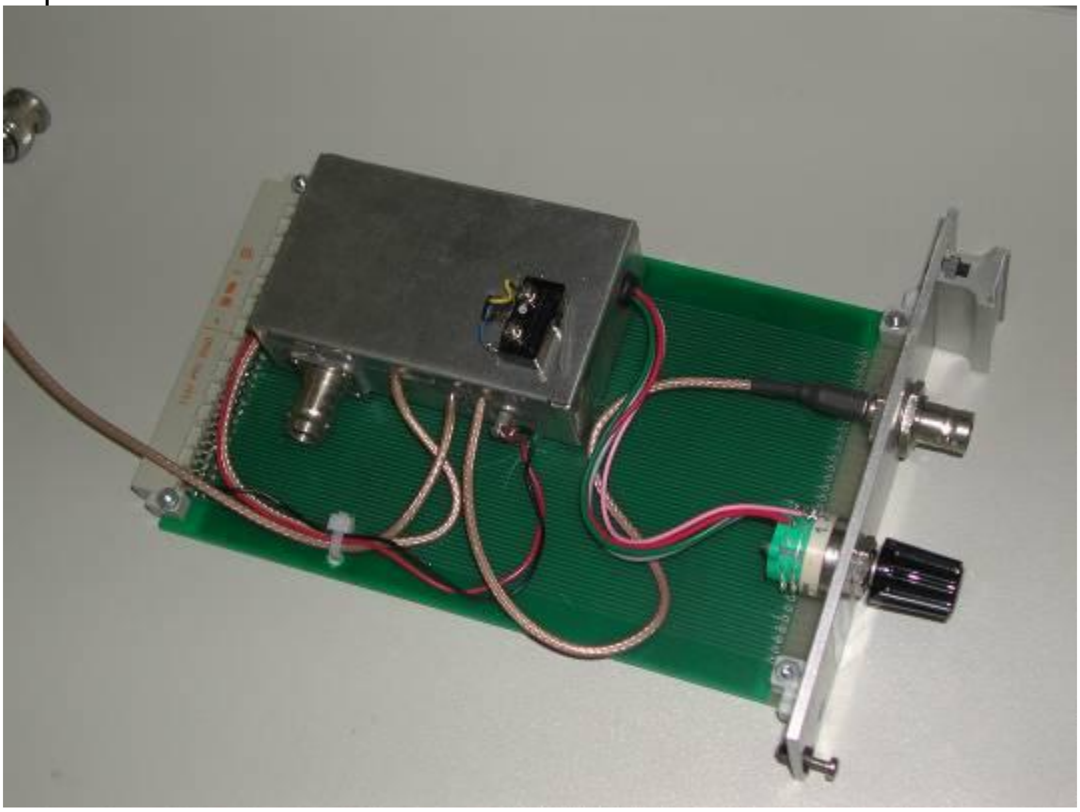

FIG.3.13 Pulse Generator Module. It is visible the micro-switch for servicing

3.2.3 Demodulator

This circuit, after a very sharp signal filtering through the above mentioned SAW filter, detects and low pass filters the received echo. The demodulated signal is sent to the oscilloscope via an additional low pass filter. This stage is supplied with a 12 V and 8 V (obtained with an internal regulator) The electric circuit is reported in Appendix. picture of the overall demodulation board is presented and FIG. 3.14. In FIG. 3.15 some more details of the demodulator hardware are visible.

3.2.4 Power Supply

The system will be supplied with 2 x 12 V batteries. A bulk switching receiver will be used in order to supply the equipment with 24 V independently from the battery charge status in the input 18 V – 27 V range. A MASCOT (Made in Norway) bulk switching power supply model8862 24/24 is used for this purpose.

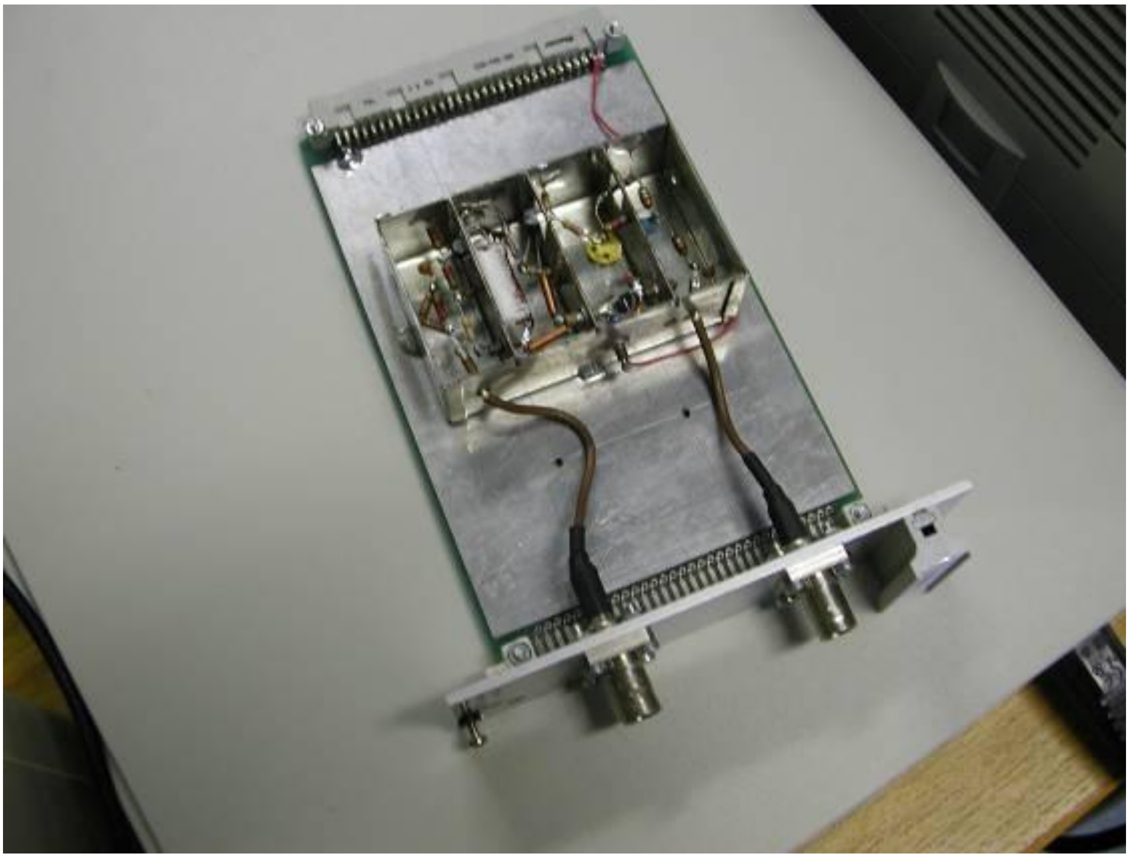

FIG. 3.14 Demodulator board

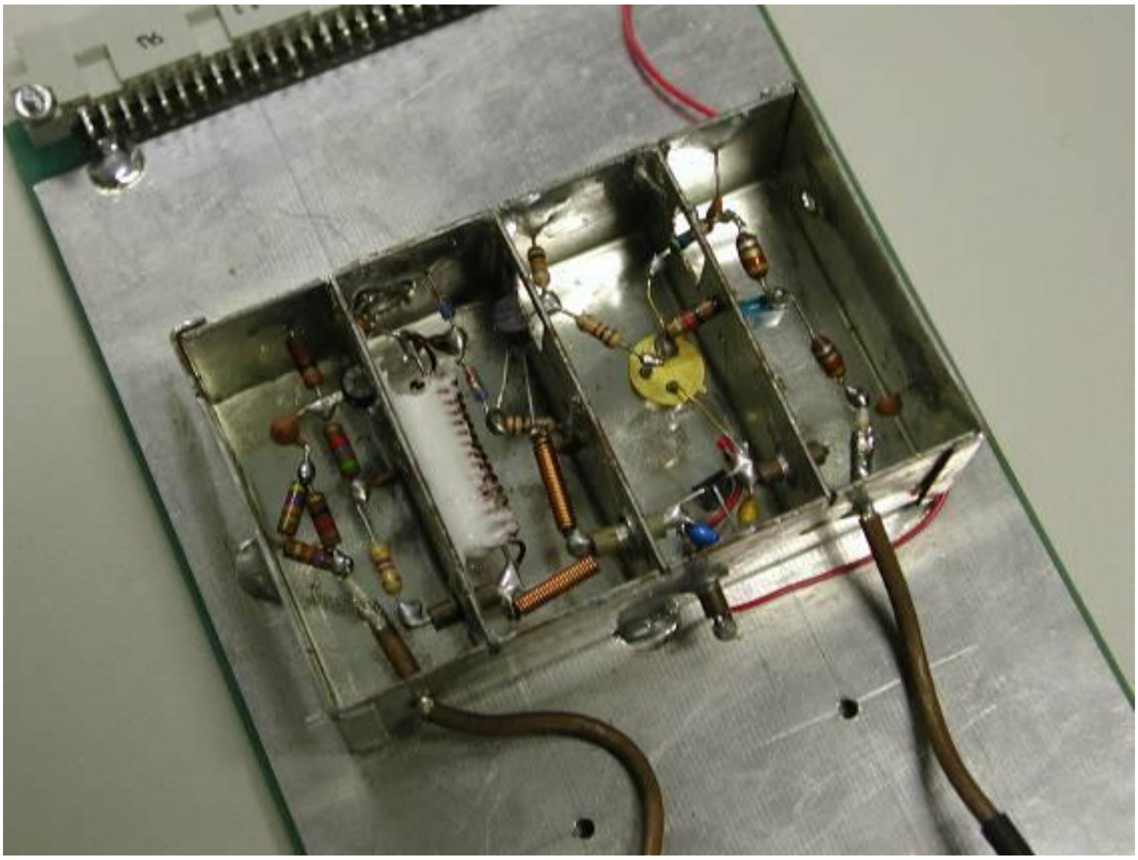

FIG. 3.15 Demodulator board details

4.0 Data Acquisition

The first version of the data acquisition system consists of a PC based oscilloscope but it will be replaced, in a near future, with a National Instr. A/D board. In that phase an ad hoc software will be written exploiting the impressive possibilities offered by the Lab-View package and the related developing environment.
At present we use a PICO ADC 200 / 20 double channels 20 Ms/sec oscilloscope. It is connected to the system as visible in FIG. 4.1

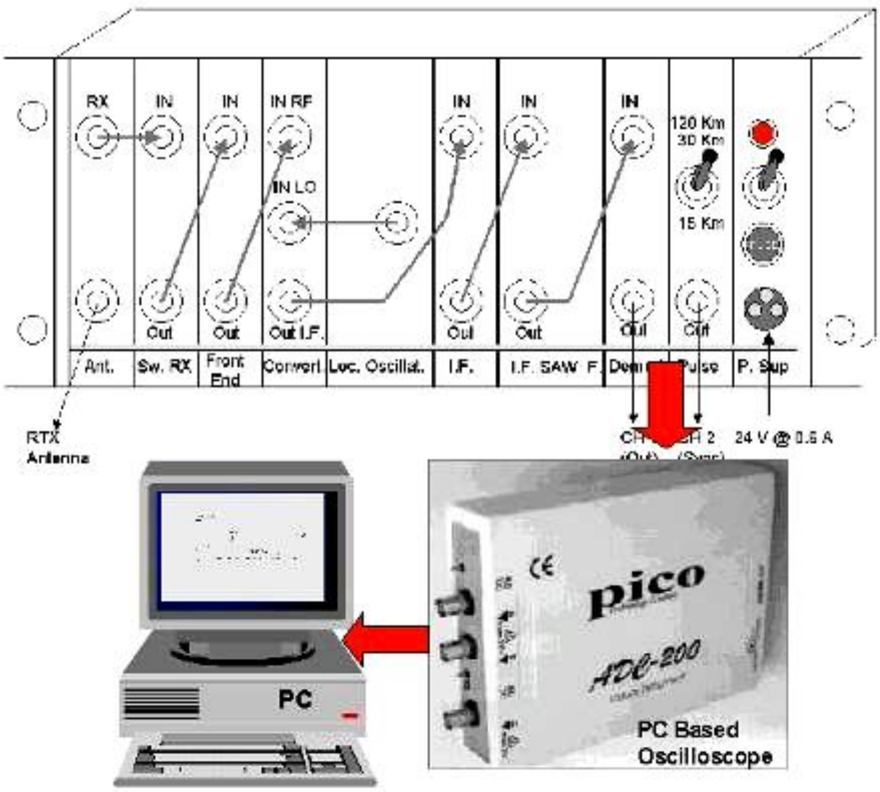

FIG. 4.1 General block diagram

The main characteristics of the PICO ADC 200 are reported below:

Pico ADC-200/20

Connects to parallel printer port of PC.

- Two channel oscilloscope 20, 50 or 100 MSamples/sec.
- 8K memory / ch. 8-bit res.
- Vin: ±50mV to ±20V. Overload: ±100V

- Voltage acc.: ±3%, time ±100ppm, 8-bit
- FFT Spectrum Analyser
- Digital display of Voltage & Freq. measurements
- In Windows, multiple display of the same input signal (eg 'Scope, Spectrum, Numerical volts and frequency)
- Oversampling for noise reduction/ resolution enhancement
- Rulers for amplitude / time measurement
- Advanced Triggering modes to catch intermittent or 'one-off' events, etc, and write to disk
- High speed data logger
- PicoScope, PicoLog & drivers for Win 3.1/95, DOS. Example code: C, Pascal; Windows: Visual Basic, Delphi, Excel
- Optional PicoScope for NT, Labview drivers, PicoLog
- Windows (3.1 or Win95) & DOS software supplied,
- Power 12V 500mA, (mains adaptor supplied)

Using the software supplied with the oscilloscope it is possible to write an ad hoc acquisition code. The acquisition software has been written in the the LabView environment (see section 8)

5.0 Antenna

In the system evaluation on the field, we are using a Yagi antenna because of the portability of such a radiator. It offers a good beam width, totally suitable for the planned uses.

The antenna employed in the test of the equipment is a 19 elements Yagi coming from the French Tonna Company. The gain is about 16.2 dB with a spatial angle (3dB) of about 28 deg. The front/back ratio is 23.56 dB. The radiation pattern is reported in FIG. 5.1

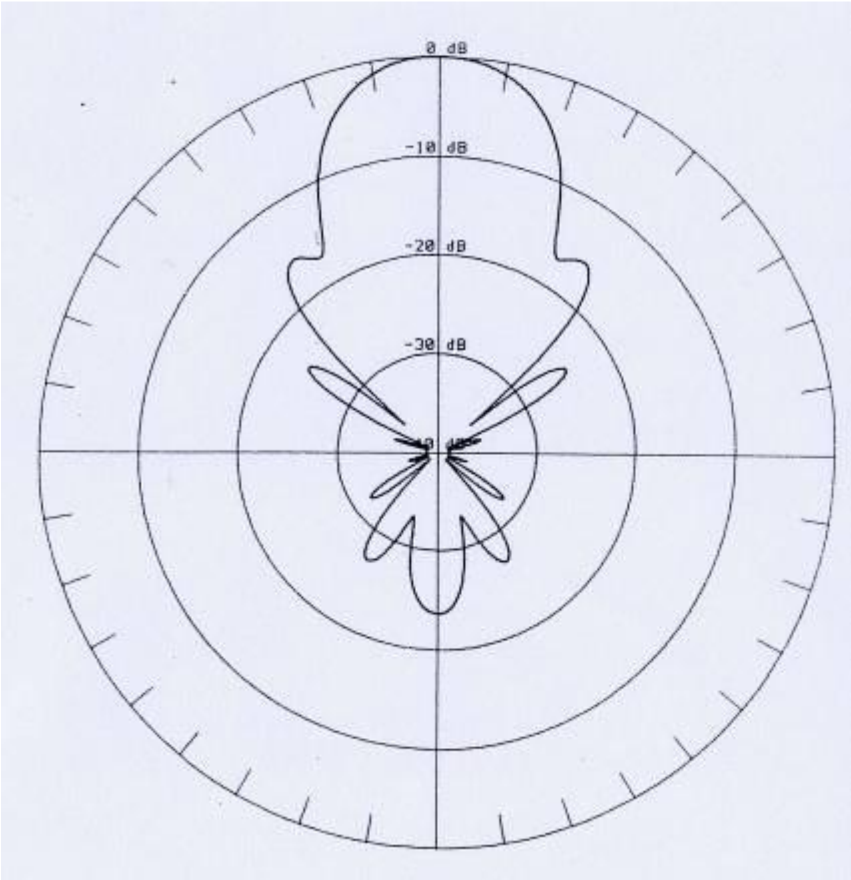

FIG. 5.1: Radiation pattern of the Tonna Yagi antenna used in the test.

The complete collection of information on the antenna correct assembling is included in the appendix section.

For applications in which the maximum achievable range is required (i.e. wind profiler or meteoroids detection), an array of the above mentioned Yagi has to be used. At each doubling of the number of antennas in the array determines the increasing of the total gain of about 3 dB. Care needs to be taken in the determination of the distance at which the antennas are mounted in order to form the array. As a first basic concept, the N antennas have to be connected at the summing point by means of equal length cables in order to sum them in phase and obtain the maximum response in the mechanically steered direction. The distance among the antennas is determined, by a thumb rule, considering the Yagi (with gain G) to have an effective equivalent "circular" area A_{eff}, with radius R (FIG. 5.2).

$$A_{eff} = \frac{G\lambda^2}{4\pi} \qquad [m^2]$$

in our case G=16.2 dB and $\lambda \approx 68.3$ cm

therefore:

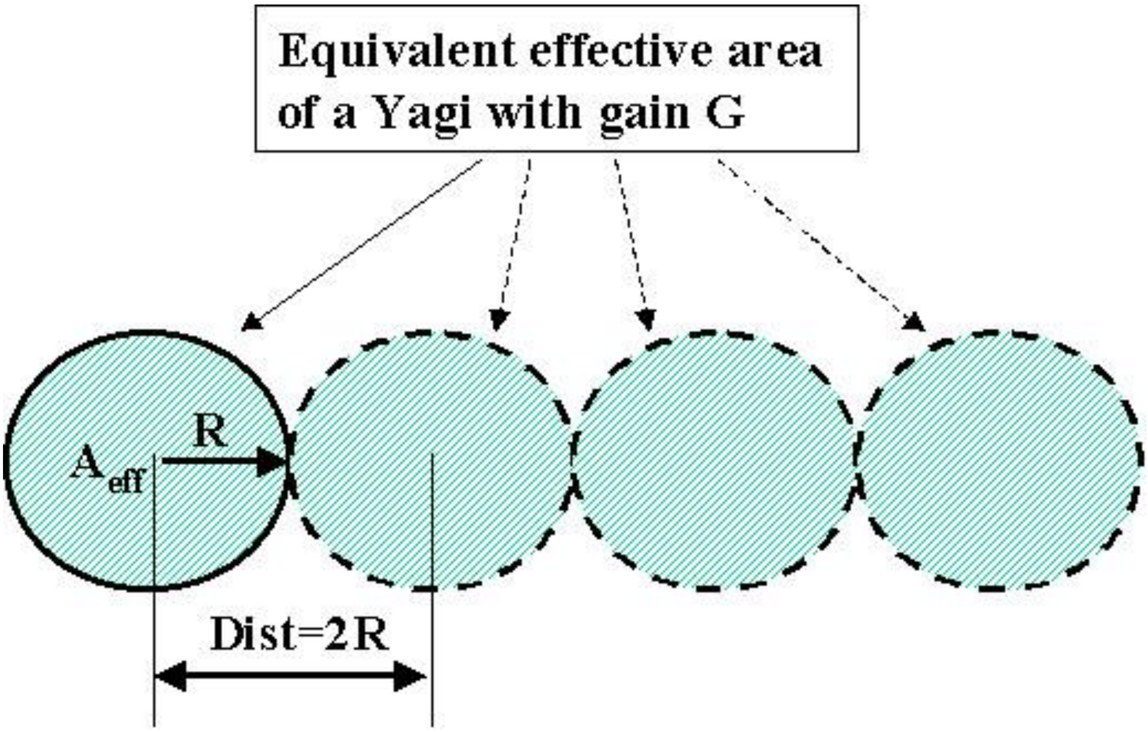

FIG.5.2 How to install several Yagi antennas in order to reduce the beam width in the horizontal plane

$$G = 10^{16.2/10} = 41.68$$

$$A_{eff} = \frac{41.68 \text{ x } (68.3)^2}{12.56} = 15480 \qquad [cm^2]$$

This corresponds to the equivalent circumference radius of:

R= 70 [cm]

So the other antenna(s) needs to be installed at

Dist.= 140 [cm]

The practical solution is sketched in FIG.5.3. In this figure it is clearly visible as the antennas are planned to be installed on the stand. As already mentioned, the cables connecting the antennas to the summing point, are requested to have the same length in order to obtain the maximum of the array pattern in the mechanically steered direction.
In our practical case, if we add 3 more antennas, as visible in the example sown in FIG.5.3, the beam width (in the vertical plane) would be reduced to 7 deg. with a gain increasing of about 6 dB (~22 dB total).

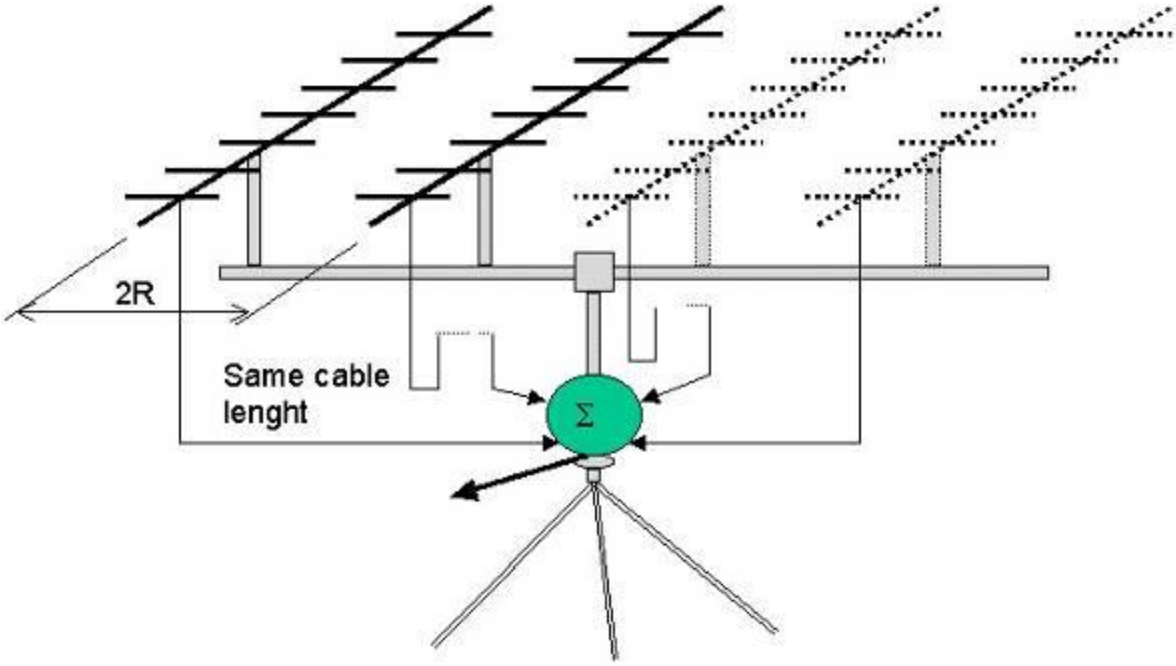

FIG. 5.3 Sketch of the antennas mounted on a stand

In the previous considerations we assumed a circular equivalent collecting area but, in the case we would reduce the vertical beam width, the distance D between the different “layers” of antennas has to be intended smaller than the computed one (2R) as visible in FIG. 5.4

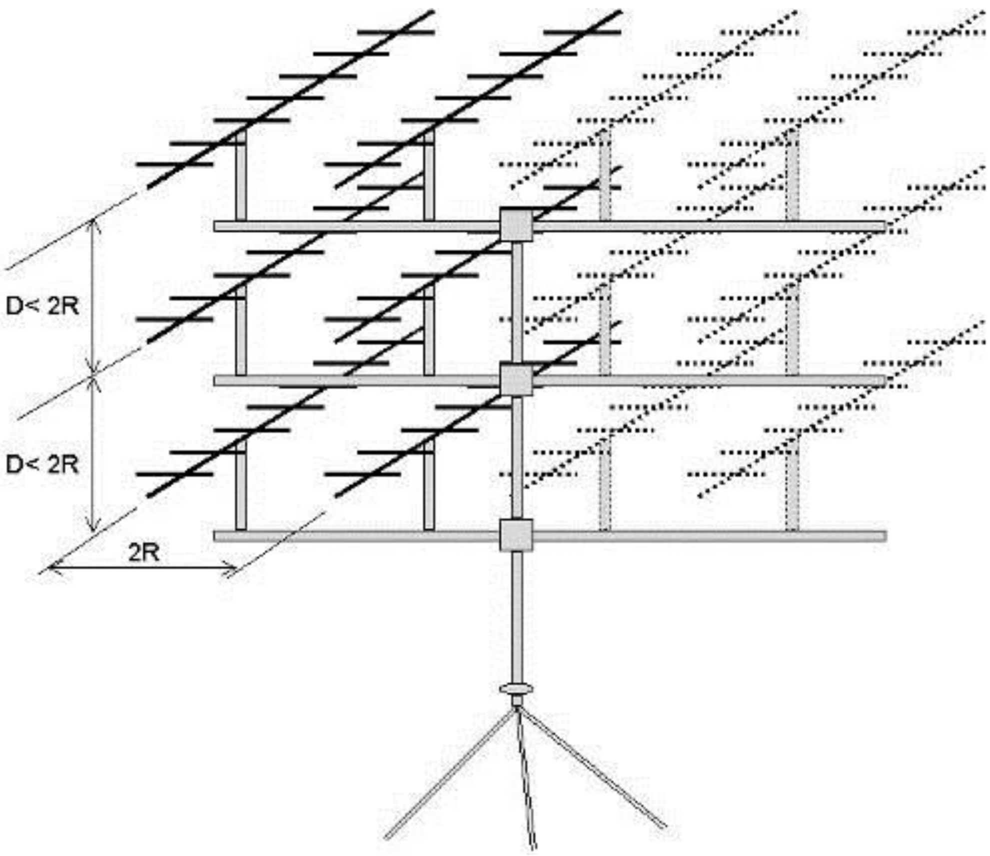

FIG. 5.4 Sketch of a multi-antennas system

A good solution is to make possible a vertical adjustment of each "*antenna layer*" inside a $\lambda/2$ range. Also in this case, all the cables (connecting the antennas to the summing point) need to have the same length. In order to connect all the elements with the proper phases, we need to be sure that the antennas come from the factory with the same *dipoles-→connectors* wiring connections sense (see FIG. 5.5).

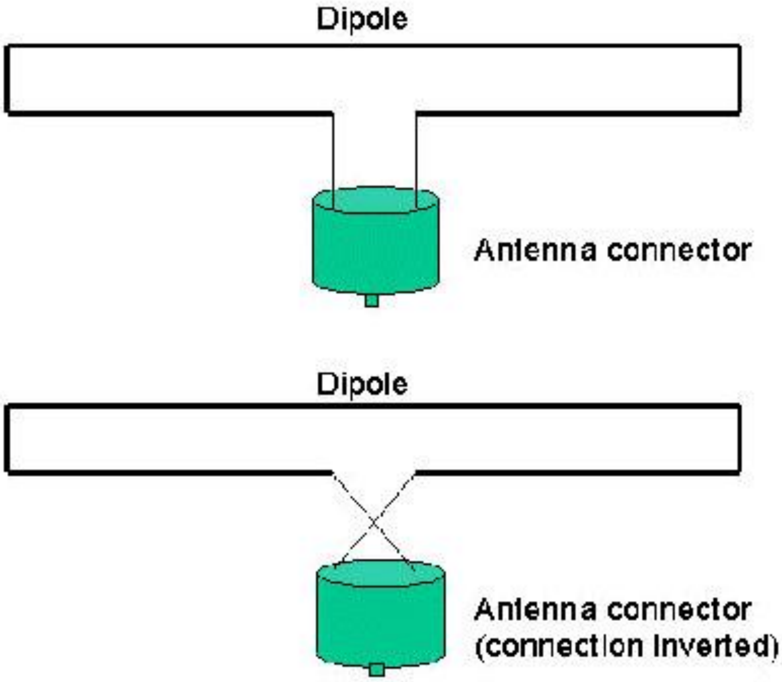

FIG. 5.5 Antenna connector internal connections

The working prototype we used for the test campaign, was composed by 3 antennas as shown in FIG. 5.6. The expected total gain is approximately 20 dB.

<u>6.0 Test</u>

A first test of the system has been performed by installing the antenna system on the institute building roof at the Medicina station (FIG:6.1). The results seem to be very promising. A lot of work has still to be done at the post processing level especially for new clutter suppression algorithms.
In FIG. 6.2 is reported the timing diagram of the system. It can be seen that the receiver is really blinded during the pulse duration (4 μsec @ 40 W). To test the system in the lab, a special test set, shown in FIG. 6.3, has to be implemented. In this test configuration, a delayed version of an amplitude programmable pulse can be generated and injected into the antenna. Using such a test configuration the system sensitivity has been evaluated at about -100 dBm.

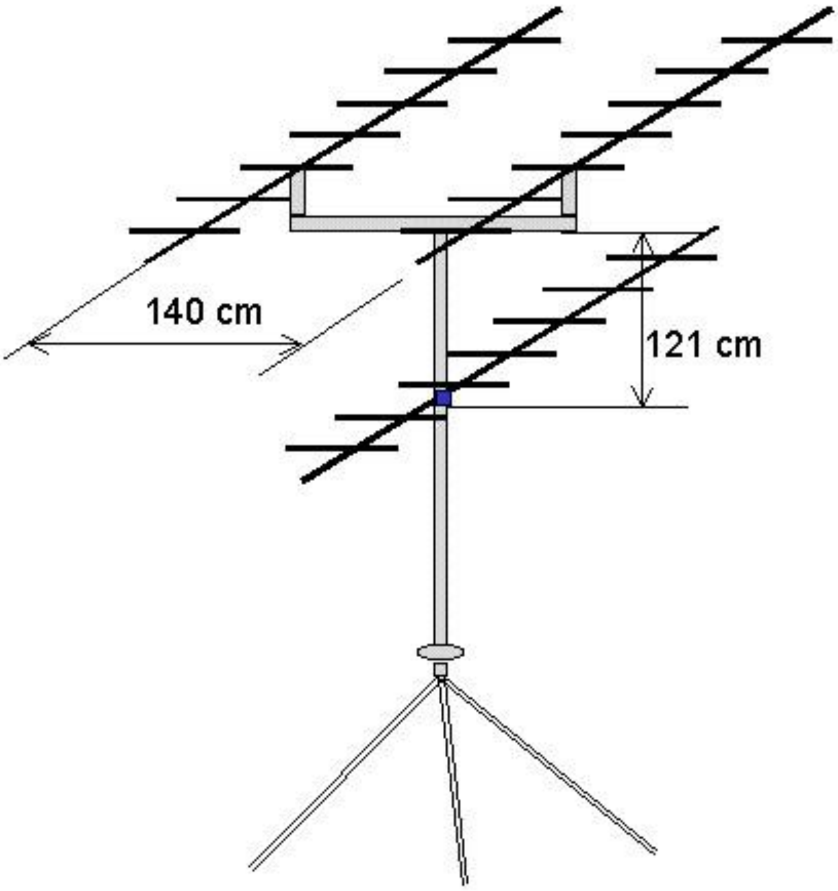

FIG.5.6 Prototype array used during tests

FIG 6.1 Test of the radar on the Institute roof

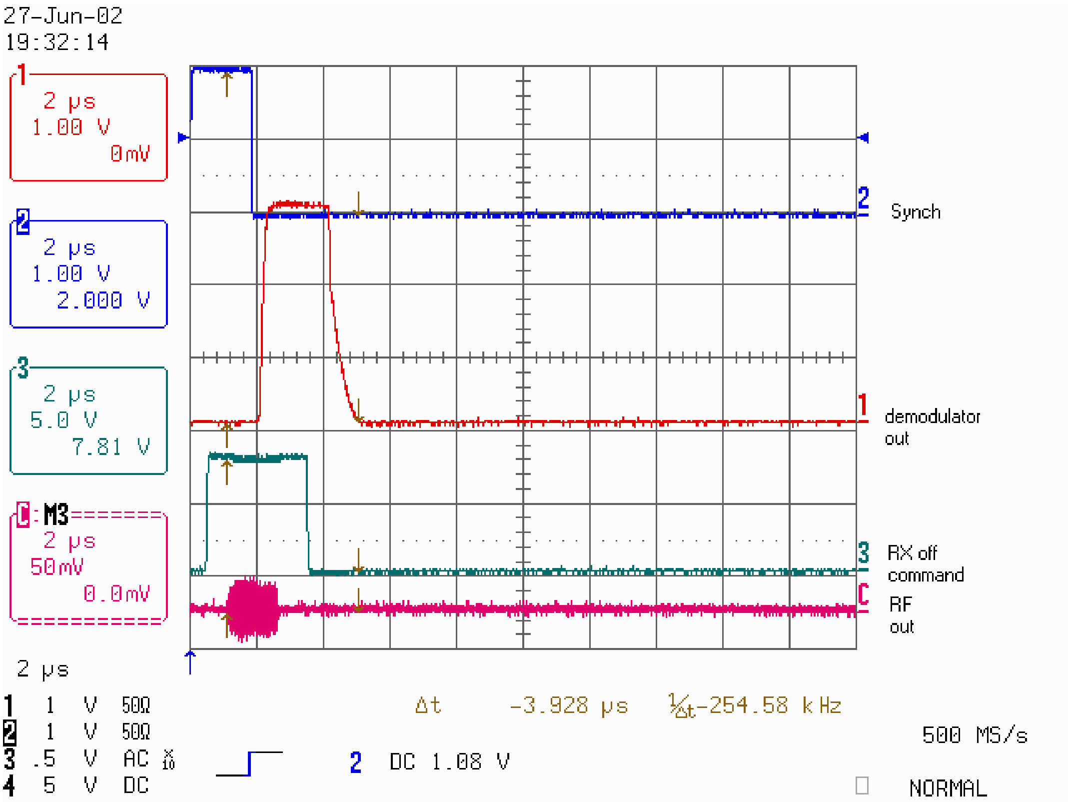

FIG. 6.2 Timing table of the system

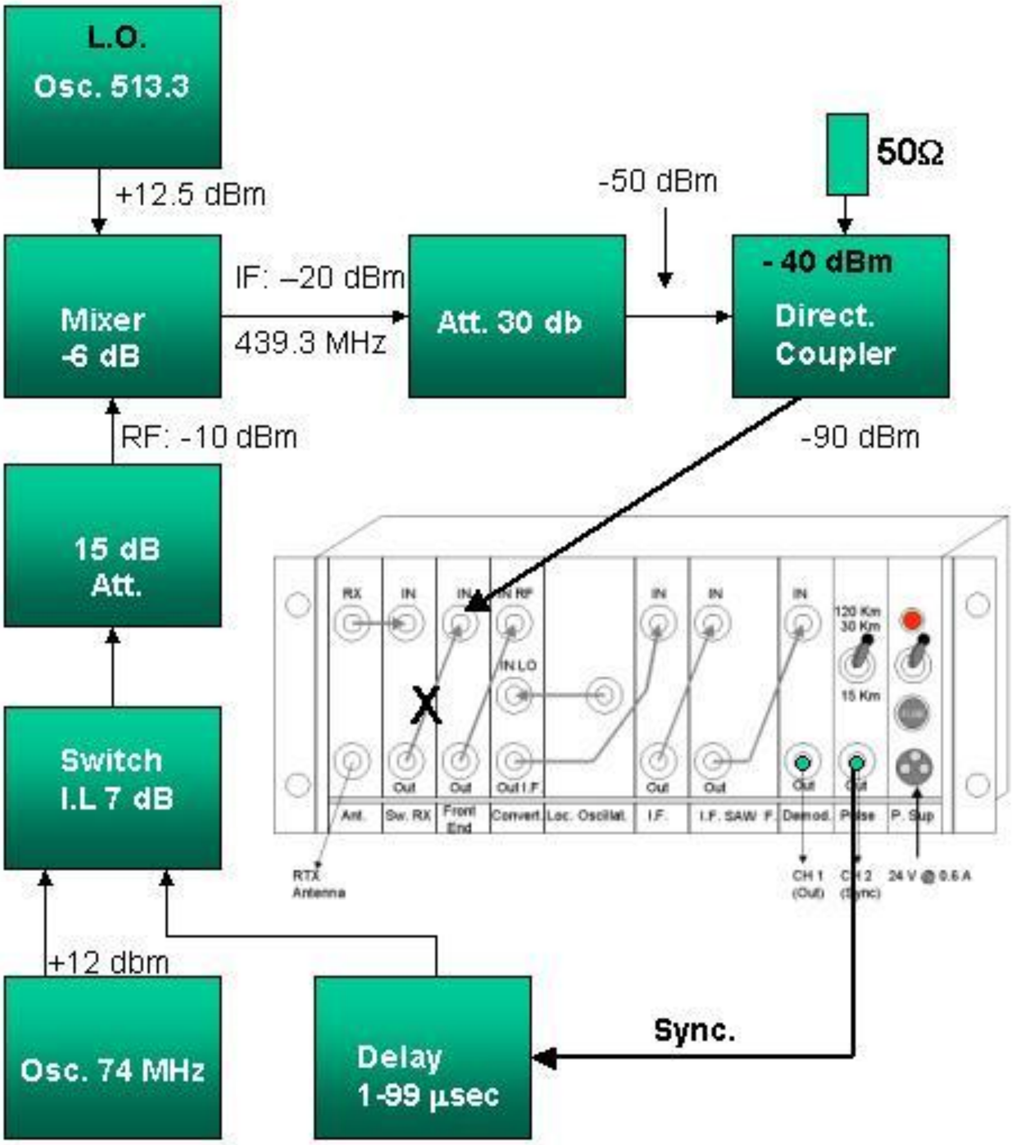

FIG.6.3 System Test Block Diagram

The internal PLL/ Multiplier connector is shown in the following wiring diagram:

Cannon Connector DB9
Oscillator & Multiplier

1	White	
2	Brown	
3	Green	
4	Yellow	
5	Grey	
6	Pink	
7	Blue	n.c.
8	Red	
9	Black	
10	Violet	n.c.

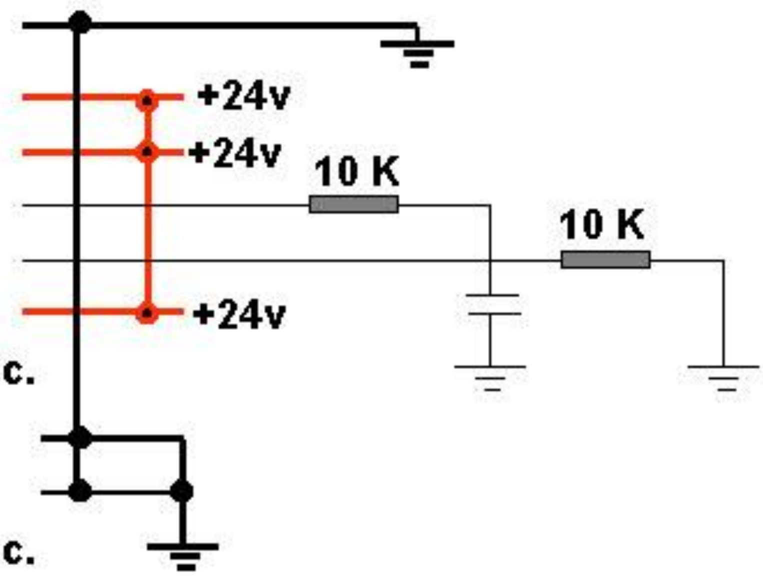

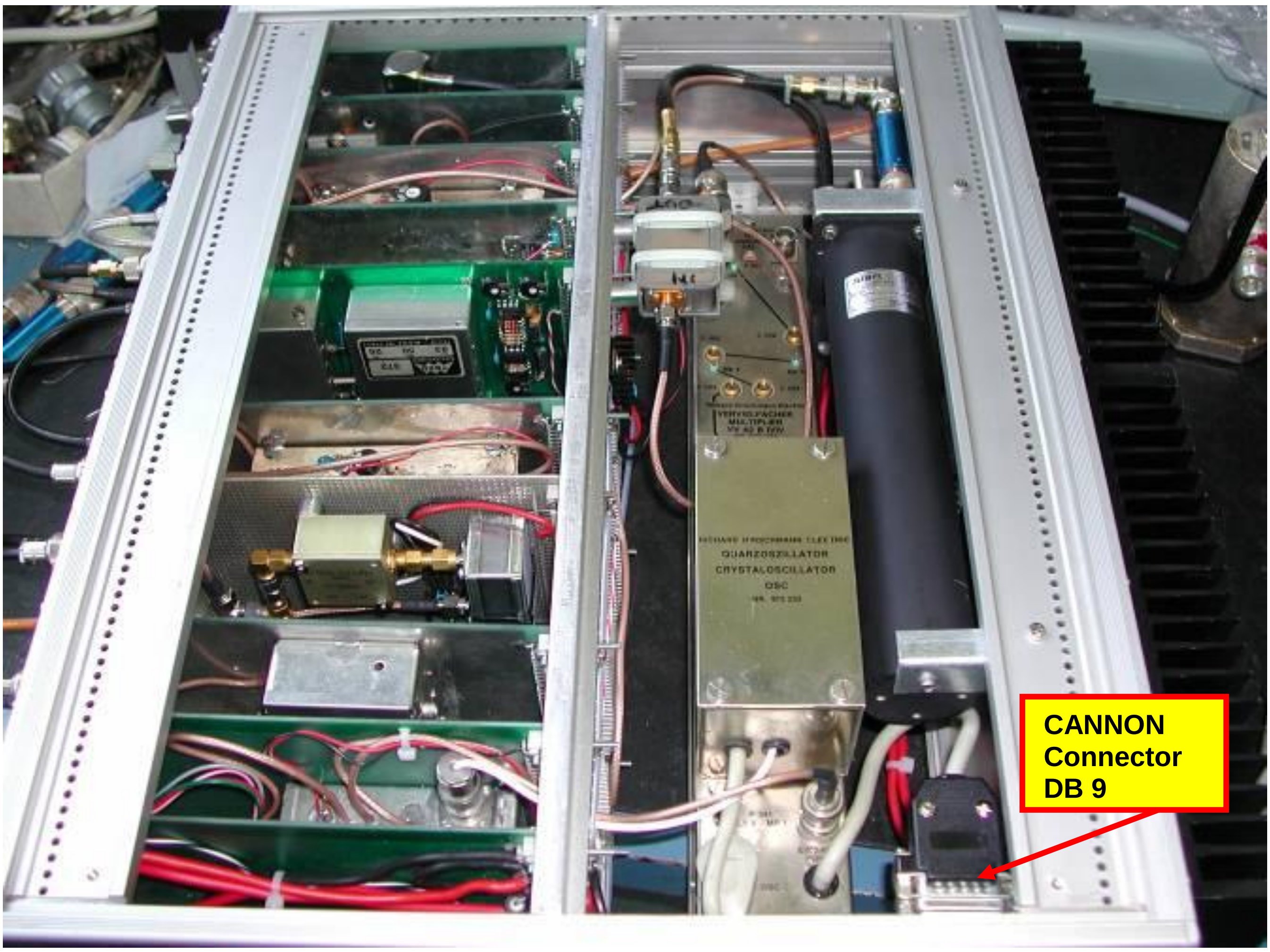

7.0 Expected Performance

The expected range of the radar (considering 20 m^2 as a minimum detectable cross section) with the following practical parameters

1. P_T= 40	W		(Transmit. Power)
2. λ= 0.683	m		(Wave length)
3. G= 20	dB	(100)	(Gain of a 3 Yagi antennas array)
4. Tsys= 300	K		(System Temperature)
5. k= 1.38 10^{-23}	JK^{-1}		(Boltzmann Constant)
6. B= 1.2	MHz		(Bandwidth)
7. SNR=10	dB	(10)	(Signal to Noise ratio)

is given by:

$$R_{\max} = \left(\frac{P_T G^2 \sigma \lambda^2}{(4\pi)^3 kTB(SNR)} \right)^{0.25}$$

$$R_{\max} = \left(\frac{40x(100)^2 x20x0.65^2}{12.56^3 x10x1.38x10^{-23} x300x1.2x10^6} \right)^{0.25} \approx 13Km$$

To increase the range or the minimum detectable Cross Section, we need to use more directive antennas. In the case of an array, this means to increment the number of the antenna elements.

8.0 Display and Acquisition software

A first display and acquisition version of the software has been written in the LabView environment. Hereafter are listed the at present test software release diagrams.

9.0 Final considerations

The radar has been housed in a very robust cabinet as visible in Fig. 9.1. This allows the use of the system on the field, under difficult environmental situations, in a safe way. The total equipment and antenna weight is about 15 Kg making it transportable in the operative area.

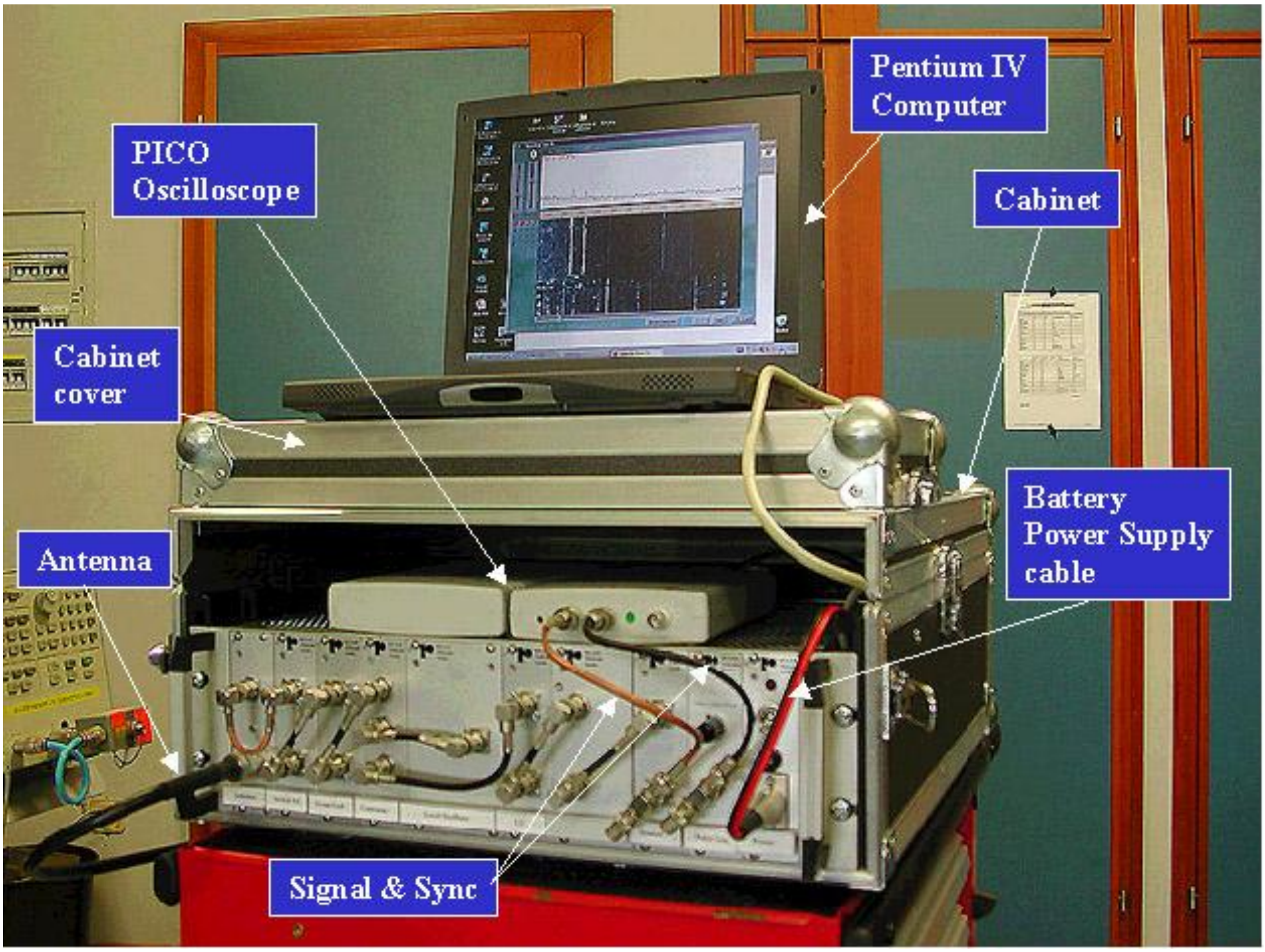

FIG. 9.1 The system housed in a robust transportable cabinet

Conclusions

After a first test on the field, the system seems to work properly. A future intensive use of such a UHF radar will inevitably lead to modifications or up grade, in order to better fit the different operative requirements. Comments and suggestions are also expected from our collaborators (***ISAC*** -Italy- and ***OCI*** –Norway-) that will use the system in different programs and conditions.

PICO
Oscilloscope Manual

APPENDIX

In this section is grouped a collection of data sheets and other general information on the devices used in the equipment. This makes easier the maintenance and, if required, the system upgrade.